Theses and Dissertations

August 2012

Decadal Changes and Future Projections of Precipitation in the Metropolitan Area of Milwaukee

Anke Petra Maria Keuser
University of Wisconsin-Milwaukee

Follow this and additional works at: https://dc.uwm.edu/etd

Part of the Climate Commons, Geography Commons, and the Water Resource Management Commons

DECADAL CHANGES AND FUTURE PROJECTIONS OF

PRECIPITATION IN THE METROPOLITAN AREA OF

MILWAUKEE

by

Anke Petra Maria Keuser

A Thesis Submitted in

Partial Fulfillment of the

Requirements for the Degree of

Master of Science

in Geography

at

The University of Wisconsin-Milwaukee

August 2012

ABSTRACT
DECADAL CHANGES AND FUTURE PROJECTIONS OF PRECIPITATION IN THE METROPOLITAN AREA OF MILWAUKEE

by

Anke Petra Maria Keuser

The University of Wisconsin-Milwaukee, 2012
Under the Supervision of Professor Dr. Woonsup Choi

This research investigated decadal changes and future projections of precipitation in the Metro Milwaukee and surrounding area, the largest urban area in Wisconsin. Spatial and temporal precipitation patterns derived for the Metro Milwaukee from the high-resolution gridded historical climatic dataset for Wisconsin were analyzed for 1950-2006. In addition, precipitation scenarios were generated via statistical downscaling of the Third Generation Coupled Global Climate Model (CGCM3) outputs. The delta method was chosen for the statistical downscaling of the CGCM3 output for the two future time periods, 2041-2070 (2050s) and 2071-2100 (2080s). The Mann-Kendall test and the Sen's slope test were applied to investigate trends of annual and extreme precipitation. The gridded historical data were interpolated with an inverse distance weighting algorithm for spatial analysis. The annual precipitation was projected to increase by 6% to 14% by the 2050s and by 8% to 12% by the 2080s. The regional analysis of annual precipitation showed that the northern regions receive less precipitation compared to the average of the study area, and the southern regions receive more. The 95th percentile of each year's daily total precipitation was projected to increase in the future. The projected changes in extreme precipitation were higher than those simulated for the annual precipitation changes. Based on the spatial patterns of annual and monthly precipitation, and the predominant wind direction, a pattern of higher precipitation amounts down-wind from the city could be observed for the historical climate dataset for 1950-2006.

TABLE OF CONTENTS

LIST OF FIGURES

LIST OF TABLES

Chapter 1: Introduction

Regional climate projections by the Intergovernmental Panel on Climate Change (IPCC) in the Fourth Assessment Report (IPCC 2007b) suggest a general increase in precipitation for most of North America during the 21st century. The ensemble mean of multi model data sets show an annual increase in precipitation for the Midwestern United States. The report on Wisconsin's changing climate, by the Wisconsin Initiative on Climate Change Impacts (2010b), projects future mean annual precipitation to increase. A significant increase in the total number of precipitation events is projected during winter and spring months (December-April) (Wisconsin Initiative on Climate Change Impacts 2011). A seasonal analysis shows a 25 percent increase in winter precipitation over most of Wisconsin. The amount of precipitation falling as rain is projected to increase significantly as well (Wisconsin Initiative on Climate Change Impacts 2011). Modeled summer precipitation outputs do not agree on how precipitation patterns will change, but the majority project a decrease of approximately five percent (Wisconsin Initiative on Climate Change Impacts 2011).

It is suggested that the expected increase in mean precipitation will have the greatest impact on urban areas, i.e. in the form of floods and flood related problems such as water pollution (Olsson et al. 2009). Most of the existing drainage systems are not capable of carrying the increased water quantity, which has large impacts on the urban environment (Olsson et al. 2009). The existing literature suggests that urban areas alter naturally occurring precipitation patterns, mainly by causing an increase in precipitation due to increased convectional precipitation as a result of large Urban Heat Islands (UHIs) (Huff and Changnon 1973). It can be speculated that projected increases in precipitation

due to climate change will be enhanced by the effects of urban areas. The increase in precipitation will have a large impact on urban environments and may lead to hazardous conditions affecting urban populations.

Most studies that addressed future changes in precipitation patterns have focused on a global and regional scale, but analyses of changes in precipitation patterns on a local and city scale have been neglected. This shows a gap in the literature addressing projected changes in future precipitatiton patterns caused by urban areas. It is necessary to further investigate how urban areas influence precipitation patterns and how future hydrological implications will affect urban environments, and the people living in cities.

Research to improve the knowledge on changes in future precipitation patterns require climate scenarios focusing on urban areas at a suitable scale. This research uses statistical downscaling to derive data with a spatial resolution that is appropriate to study urban precipitation changes.

The main objective of this research is to investigate decadal changes and future projections of precipitation in the Metro Milwaukee and the surrounding area. The main objective will be addressed through the following two aims:

1) Spatially and temporally analyze precipitation for the time period 1950-2006 in the Metropolitan area of Milwaukee, Wisconsin

2) Generate precipitation scenarios via statistical downscaling of global climate model outputs.

The central hypothesis is that urban-enhanced precipitation will strengthen under global climate change. An increase in the Urban Heat Island effect is expected to further intensify changes in precipitation patterns, frequency, and intensity. This research will

improve our understanding on how urban areas will influence future changes in precipitation patterns, and will help to develop better urban hydroclimatic simulations. In addition, it adds further knowledge to the already existing research on precipitation changes in Wisconsin, and provides a more detailed analysis of the largest urban area in Wisconsin, the metropolitan area of Milwaukee.

Chapter 2: Literature Review

2.1 Precipitation Changes in Wisconsin

Based on state averages given by the Midwestern Regional Climate Center (2009), the annual mean precipitation for the state of Wisconsin has increased by 56 mm from 1895 to 2006. An increase in precipitation was also observed for the mean spring precipitation, the mean summer precipitation, and the mean autumn precipitation (Midwest Regional Climate Center 2009). While state-level assessments of precipitation are important, climate change does not occur in homogenous spatial patterns throughout whole states and very often differ in magnitude and direction over larger areas. Therefore, more detailed analyses are necessary.

Kucharik et al. (2010a) analyzed the patterns of climate change across Wisconsin from 1950 to 2006 based on observational data. Kucharik et al. (2010a) found an increase in annual average precipitation by approximately 5 to 15% (50-100 mm) with a statewide average of 79 mm. The spatial variation of mean annual precipitation shows the highest increases in the west-central and the south-central regions. The northwest and north-central regions experienced decreasing precipitation trends (Kucharik et al. 2010a).

Seasonal precipitation trends showed an increase in winter precipitation of 10 to 20 mm across most of Wisconsin. The observed trends were weak and are only at a few isolated grid points of significance. The spring-time precipitation also shows increasing trends (20 to 60 mm) for the southern and western portions of Wisconsin. Again, the majority of the trends were of no significance (Kucharik et al. 2010a). Summer precipitation also has increased from 30 to 60 mm for the southern parts of Wisconsin, and only a small portion of this area (central corridor from north to south) is significant.

A small part of the southeast corner of Wisconsin, just below Milwaukee County, shows a significant trend towards less precipitation. Similar trends can also be observed across the northern third of the state (Kucharik et al. 2010a). The average fall precipitation increases by approximately 48 mm with significant trends in the northwestern corner of Wisconsin (Kucharik et al. 2010a).

The Wisconsin Initiative on Climate Change Impacts present projected precipitation for the mid and late 21st century (2046 – 2065 and 2081 – 2100) based on statistical downscaling results of the global climate models that were used for the World Climate Research Programme's (WCRP's) Coupled Model Intercomparison Project phase 3 (CMIP3) (Kucharik et al. 2010b). Results for the A1B emission scenario suggest that the average annual precipitation for Wisconsin will change by -5% to +15% by mid 21st century and -5% to +25% for late 21st century. A seasonal analysis based on the A1B scenario shows that precipitation is projected to increase in winter (0 to 40%), and fall (5% to 15%). No agreement could be found for summer but the modeling results suggest a change between -20% and +15%. During spring the projected change is of -5% to +25% (Kucharik et al. 2010b). The modeled results also suggest that heavy precipitation will increase for Wisconsin, especially in the eastern and northern regions.

2.2   Effects of Urban Areas on Precipitation

In the second half of the 20th century, studies have theorized that the Urban Heat Island (UHI) can alter mesoscale convectional circulation which results in changes of precipitation patterns (Huff and Changnon 1973; Changnon, Semonin, and Huff 1976; Changnon 1981; Changnon and Huff 1986; Huff and Changnon 1986; Changnon, Shealy, and Scott 1991; Shepherd, Pierce, and Negri 2002; Dixon and Mote 2003; Shepherd

2005). Dixon and Mote (2003) analyzed the effect of Atlanta's UHI on the temporal and spatial patterns of precipitation, i.e. when and where precipitation events occur. The UHI in Atlanta has shown to enhance or even initiate thunderstorms resulting in increased precipitation on the downwind side of the city (Dixon and Mote 2003). Furthermore, the results of the study suggest that the majority of urban induced precipitation events occurred within 5-10 km from areas of major urban development. Low level moisture contents in the atmosphere seemed to be more important than the UHI intensity (Dixon and Mote 2003).

Huff and Changnon (1973) analyzed the urban effects on precipitation in eight major cities (St. Louis, Chicago, Indianapolis, Cleveland, Washington, Houston, New Orleans, and Tulsa) and their surroundings in the central and eastern United States. For the time period 1955 to 1970, urban-induced increases in precipitation were found for the daily and seasonal precipitation for St. Louis, Chicago, Washington D.C., and Cleveland. In Houston and New Orleans urban effects were only detected in increased warm season rainfall caused by air masses. Evidence for Tulsa and Indianapolis was weak or non-existing. The urban effect seemed to be more pronounced on the downwind side of the central city (Huff and Changnon 1973).

The UHI does not necessarily initiate precipitation occurrences, but rather acts as an enhancing factor, and most events occur during the night and near high-density urban areas (Changnon 1981). Results from the Metropolitan Meteorological Experiment (METROMEX) also show that the number of precipitation events did not increase, only an increase in the amount of precipitation was observed (Changnon 1981).

2.3   Climate Scenarios

In any project including future climate change a thorough analysis including averages, variability, and mean of current climate conditions should be included. Such an analysis is required to understand the current climate system and the significance of projected future changes (Barrow and Lee 2000). As defined by the World Meteorological Organization (WMO), the current climate, also known as the reference or baseline climate, generally refers to a 30-year normal period (Mitchell et al. 1966) and is derived from historical climate observations (Barrow and Lee 2000; Carter et al. 2007). A popular climatological approach to defining the baseline period is to use the non-overlapping 30-year normal period from 1961-1990 as defined by the WMO (IPCC 2007a).

According to Carter et al. (1994) a climate scenario is defined as, "a coherent, internally-consistent and plausible description of a possible future state of the world." A scenario is a plausible future based on a quantified description of future climates, which are consistent with assumptions of future greenhouse gas emissions and other pollutants and with the assumptions on how these changes in concentration of greenhouse gasses will affect global climate (Carter et al. 2007). Climate scenarios ideally consist of a set of multiple scenarios and encompass a range of likely future developments (Smith and Hulme 1998). Three generic types of climate scenarios exist: synthetic scenarios, analogue scenarios, and scenarios based on outputs from global climate models. All of these scenarios have been used in climate impact studies; the majority of studies are based on climate change scenarios from global climate models (Smith and Hulme 1998; Carter et al. 2007). Climate scenarios based on global climate model outputs are currently

the most credible tool to develop future climate scenarios (Barrow and Lee 2000). Before climate change scenarios are generated, it is important to address changes of those atmospheric conditions that will cause changes in climate.

2.3.1 Emission Scenarios

In order to address future changes of atmospheric conditions for the next 100 years it is necessary to construct greenhouse gas emissions for the 21st century (Carter et al. 2007). These scenarios are used in GCMs to simulate changes in climate and are based on assumptions on the development of societal activities in the future.

Before issuing the Third Assessment Report (IPCC 2007b) the IPCC commissioned a Special Report on Emission Scenarios (SRES) (Nakicenovic et al. 2000) in which the most recent emission scenarios can be found. The scenarios, as described in the SRES (Nakicenovic et al. 2000), are based on an extensive assessment of driving forces and emissions of greenhouse gasses in the scenario literature.

Four different narrative storylines (A1, A2, B1, B2) were developed based on assumptions on how society will evolve in the 21st century and beyond. Each storyline is based on different demographic, social, economic, technological, and environmental developments and include a large variety of main demographic, economic, and technological driving forces of greenhouse gasses and sulfur emissions. Feedback effects of future climate change on emissions from energy and biosphere are not included in the scenarios. Based on these storylines four so called 'families' have been identified (Nakicenovic et al. 2000).

The associated storylines entail following key assumptions (Nakicenovic et al. 2000):

• The A1 storyline and scenario family describes a future world with a steep population growth that peaks in the 1950s and rapidly declines thereafter with rapid economic growth, reduction in regional differences in per capita income, and development of new and more efficient technologies.

• The A2 storyline and scenario family looks at a diverse and heterogeneous world with a steady population growth (ca.15 billion by 2100) and emphasis on regional economic growth. A more fragmented and slower economic growth and technological change than in other storylines is predicted.

• The B1 storyline and scenario family assumes a convergent world with a population that peaks in the 2050s and subsequently declines, similar to the A1B scenario, reaching ca. 7 billion by 2100. Economic structures are rapidly developing in a service and information economy with an emphasis on clean and efficient technologies due to a global concern for social and environmental sustainability.

• The B2 storyline and scenario family is a world where local solutions to economic, social and environmental sustainability are emphasized. This world is characterized by a steadily growing population, (at a lower rate than the A2 scenario family), intermediary economic development, and a more diverse but slower developing technological change than in the B1 and A1 storylines.

The existing scenarios span a wide range of future economic development and activity, as well as different trends in population growths. In the IPCC Special Report on Emissions Scenarios (Nakicenovic et al. 2000) it is recommended that multiple emission scenarios are used in any analysis regarding future climate change. There is no single most likely or 'best-guess' scenario, and likelihoods are not assigned to SRES scenarios.

2.3.2 Global Climate Models

Global climate models (GCMs) represent the physical processes of the atmosphere, ocean, cryosphere, and land surface, and are currently the most credible tool for developing climate scenarios (Barrow and Lee 2000; Carter et al. 2007). GCMs are numerical models that simulate large-scale physical processes of the earth atmosphere and ocean system (Fuentes and Heimann 2000). These models have been derived based on well-established physical principles and then approximated through mathematical discretization to project past, current, and future climate (IPCC 2007b). GCMs depict climate for a three dimensional grid with a horizontal resolution between 250 to 600 km, and a vertical resolution of 10 to 20 vertical layers into the atmosphere, and can have as many as 30 layers down in the ocean (Smith and Hulme 1998; Carter et al. 2007). The most sophisticated GCMs available are the coupled atmosphere-ocean general circulation models (AOGCM). These GCMs are comprised of an atmospheric general circulation model (AGCM) coupled to an ocean general circulation model (OGCM) (Carter et al. 2007). The AGCM is a three dimensional representation of the atmospheric layers coupled to the land surface and cryosphere layers. The OGCM is a three dimensional representation of the oceans and sea-ice (IPCC 2007b). Data from many different GCMs developed around the world are provided by the Intergovernmental Panel on Climate Change Data Distribution Center (http://www.ipcc-data.org/index.html).

One major disadvantage of GCMs is that despite the accurate representation of global climate, their simulation of regional climate is often inaccurate (Smith and Hulme 1998). Another disadvantage of GCMs is their coarse geographic and temporal scale, which is often not fine enough for impact studies. Within GCMs, represented as gridded

datasets, with a spatial resolution of hundreds of kilometers, each grid box represents uniform climate changes. Although the temporal resolution of GCMs estimate climate on a daily or sub-daily (mostly twice a day) basis, the results are generally archived on a monthly time series (Barrow and Lee 2000). Daily GCM data are freely available only for very few GCMs, e.g. the third generation coupled global climate model.

To overcome the gap between the large spatial resolution of GCMs and the much finer resolution needed for impact studies, downscaling methods that create finer resolution datasets have been developed. Downscaling techniques have emerged to interpolate planetary scale atmospheric predictor values to smaller scale meteorological series (e.g. regional or local scale) (Wilby and Wigley 1997). The simplest downscaling option is to interpolate the GCM outputs to a finer, smaller scale. More complex methods can be grouped into dynamical downscaling, and statistical downscaling methods.

2.3.3   Dynamical Downscaling

Dynamical downscaling, also known as nested downscaling, uses the large-scale GCM to extract local-scale information by creating Limited-Area Climate Models (LAMs) or Regional Climate Models (RCMs) with a spatial resolution of tens of kilometers (most often 20-50 km) (Wilby and Wigley 1997; Xu 1999; Xu, Widen, and Halldin 2005). Dynamical downscaling nests a RCM into a GCM to model the physical and dynamical processes of the GCM with a smaller resolution for a defined area (Maraun et al. 2010). This method uses the GCM to provide the initial and time-dependent lateral boundaries to simulate large scale atmospheric circulation, and the

surface boundary conditions to drive the high resolution RCM and capture smaller scale atmospheric variability (Xu, Widen, and Halldin 2005).

Recently, dynamical downscaling methods have been significantly improved by combining multiple nesting and atmospheric RCMs, with lake and hydrology models (Xu, Widen, and Halldin 2005). Despite these improvements several limitations to this approach still exist. The selection of the underlying GCM is very important, as the RCM simulations are strongly influenced by any deficiencies in the GCM. As the RCM uses the boundary conditions of the GCM, any biases within the GCM will be transferred to the RCM which complicates the evaluation of the RCM itself (Wilby and Wigley 1997). Depending on the size of the domain, as well as the spatial and temporal resolution, RCM simulations can be computationally demanding and costly. Often times, the spatial resolution of 20-50 km is too large for impact studies and downscaling to smaller scales or individual sites is necessary (Wilby and Wigley 1997; Xu, Widen, and Halldin 2005).

2.3.4   Statistical Downscaling

Statistical downscaling (or empirical downscaling) methods are based on finding empirical relationships between large-scale climate information (predictors) and local or regional meteorological variables (predictands) (Xu 1999; Wilby et al. 2004; Hanssen-Bauer et al. 2005). Maraun et al. (2010) describes statistical downscaling as a kind of mapping between the predictor (X) and the expected value E of the observational data (Y) based on a vector of unknown parameters (β) and given in the following equation (1):

$$E(Y/X) = f(X, \beta) \tag{1}$$

The majority of downscaling studies have used daily mean temperature or daily total precipitation as observational data. However, any high quality, long-term observational climate variable can be used as long as it makes sense to use this variable for the climate study (Hanssen-Bauer et al. 2005; Maraun et al. 2010). The large-scale atmospheric variables are most often obtained from GCMs at a monthly or daily temporal resolution.

The simplest downscaling method is to apply the large-scale GCM projections in the form of change factors (CFs) by applying the differences between the control and future GCM simulations to the baseline observation. This is achieved by scaling the mean and adding the resulting climatic CF to each day. This method is referred to as the 'change-factor method', 'pertubation-method' or 'delta change approach' (Prudhomme, Reynard, and Crooks 2002; Fowler, Blenkinsop, and Tebaldi 2007). This method can be easily applied to several GCMs, and is computationally fast and inexpensive, but it assumes that the GCMs simulate relative changes more accurately than absolute values, and therefore assume a constant bias through time (Fowler, Blenkinsop, and Tebaldi 2007).

More sophisticated statistical downscaling techniques are often grouped in three main categories based on the underlying technique that is being used (Wilby et al. 2004; Fowler, Blenkinsop, and Tebaldi 2007): regression-based models, weather pattern based models, and stochastic weather generators.

Regression-based models are based on quantitative relationships between large-scale variables and local/regional surface variables. This method uses statistically based models to determine the statistical linear or non-linear relationship between the large

scale atmospheric forcing (predictor) and the predictands through a regression function (Fowler, Blenkinsop, and Tebaldi 2007). More complex methods model the mean and variability by linking the covariance of the GCM with that of the predictands in a bilinear way. Other successfully applied methods include multiple regression models, canonical correlation analysis (CCA) and artificial neural networks (ANN) (Wilby and Wigley 1997; Wilby et al. 2004; Maraun et al. 2010). One main assumption is made within these transfer function methods; the GCM variables (predictors) fully include the climate change signals and are realistically modeled by the GCM. These methods are relatively straight forward to apply and are computationally and cost wise less demanding than other downscaling methods (Wilby et al. 2004; Maraun et al. 2010).

Weather pattern based downscaling groups days with regional or local variations within the selected variables based on their synoptic similarities into a finite number of weather types, or so called states (Wilby et al. 2004). Most commonly, weather types are defined by applying subjective circulation classification schemes or by using a cluster analysis of atmospheric fields (Wilby et al. 2004). Both approaches group weather patterns based on their similarity either by a nearest neighbor approach, or a reference set. After groups of weather patterns are established, the small scale variable is assigned to the appropriate weather pattern and replicated under future climate conditions through regression functions or resampling (Wilby et al. 2004). Weather pattern based downscaling methods are dependent on the quality of the weather classification and might be insensitive to future climate forcing (Wilby et al. 2004).

Stochastic weather generators are statistical models that generate random sequences of weather data (commonly of multiple variables) that have similar statistical

properties as the observed weather data at a daily or sub-daily scale (Wilks and Wilby 1999; Maraun et al. 2010). The future climate is generated by altering the parameters of the weather generator based on the predicted changes in climate from a GCM (Semenov and Stratonovitch 2010). The focus of most weather generators is on producing precipitation series that are based on occurrence and intensity (Maraun et al. 2010). The occurrence of precipitation is expressed in two different states, wet or dry. The precipitation amount is focused on non-zero amounts and is often skewed towards lower numbers as there are many more occurrences with small precipitation amounts and only a few with large amounts of precipitation (Wilks and Wilby 1999). Maximum and minimum temperatures as well as solar radiation are very often generated besides precipitation indices (Wilks and Wilby 1999). Weather generators produce large ensembles for multiple climate variables (Wilks and Wilby 1999).

While statistical downscaling methods are comparatively cheap, computationally efficient, and can provide climatic variables at point-scale that are derived from the GCM-scale, long-term and reliable historical observation data series are needed for the calibration (Fowler, Blenkinsop, and Tebaldi 2007). The statistically downscaled data is derived based on a statistical relationship between the large-scale predictors and the local-scale predicands. Therefore, the statistical downscaling process is dependent on the choice and quality of the predictors (Fowler, Blenkinsop, and Tebaldi 2007). Predictors should be physically meaningful and reproduced well by the GCM, and should be able to reflect processes responsible for climatic variability for various timescales. In addition, the predictor-predictand relationship is assumed to be the same in the future as it is for the current time period. This assumption is questionable in observed records (Fowler and

Kilsby 2002) and it is suggested that long records or model validations are used to test this for a period with different climate characteristics (Fowler, Blenkinsop, and Tebaldi 2007). Another concern is that climate system feedbacks are not included, and therefore the true extent of changes might not be captured (Fowler, Blenkinsop, and Tebaldi 2007).

Chapter 3: Study Area

The study area encompasses Milwaukee County, and a roughly drawn 24 km buffer around it. Milwaukee County has been selected to be representative of the urban area and will be referred to as Metro Milwaukee. According to the U.S. Census Bureau a metropolitan area, also referred to as metro area, is defined as an area that contains a core urban area with a population 50,000 or more and can be comprised of one or more counties. Often times, where a high degree of social and economic integration of the core urban area with adjacent counties exists, these adjacent counties are included in the metro area as well (http://www.census.gov/population/metro/).

The 'Metropolitan area of Milwaukee', or 'Metro Milwaukee', as identified by the U.S. Census Bureau, is comprised of the following 5 counties: Milwaukee, Waukesha, Racine, Washington, and Ozaukee. Looking at the land cover for Metro Milwaukee, as identified by the U.S. Census Bureau, it becomes evident that this large area is not only comprised of urban land-cover.

For the purpose of this project only Milwaukee County is included in Metro Milwaukee; the other four counties (Waukesha, Racine, Washington, and Ozaukee) have not been included. This decision was based on the analysis of land-cover data for Metro Milwaukee as defined by the U.S. Census Bureau. Within this area not only urban land-cover but large stretches of vegetation, agricultural fields and wetlands are included as well. In order to analyze if the urban area has an impact on precipitation, a metro area comprised of urban land-cover has to be identified. Milwaukee County has been selected as the metro area (Metro Milwaukee) because this area is mainly comprised of urban-land cover.
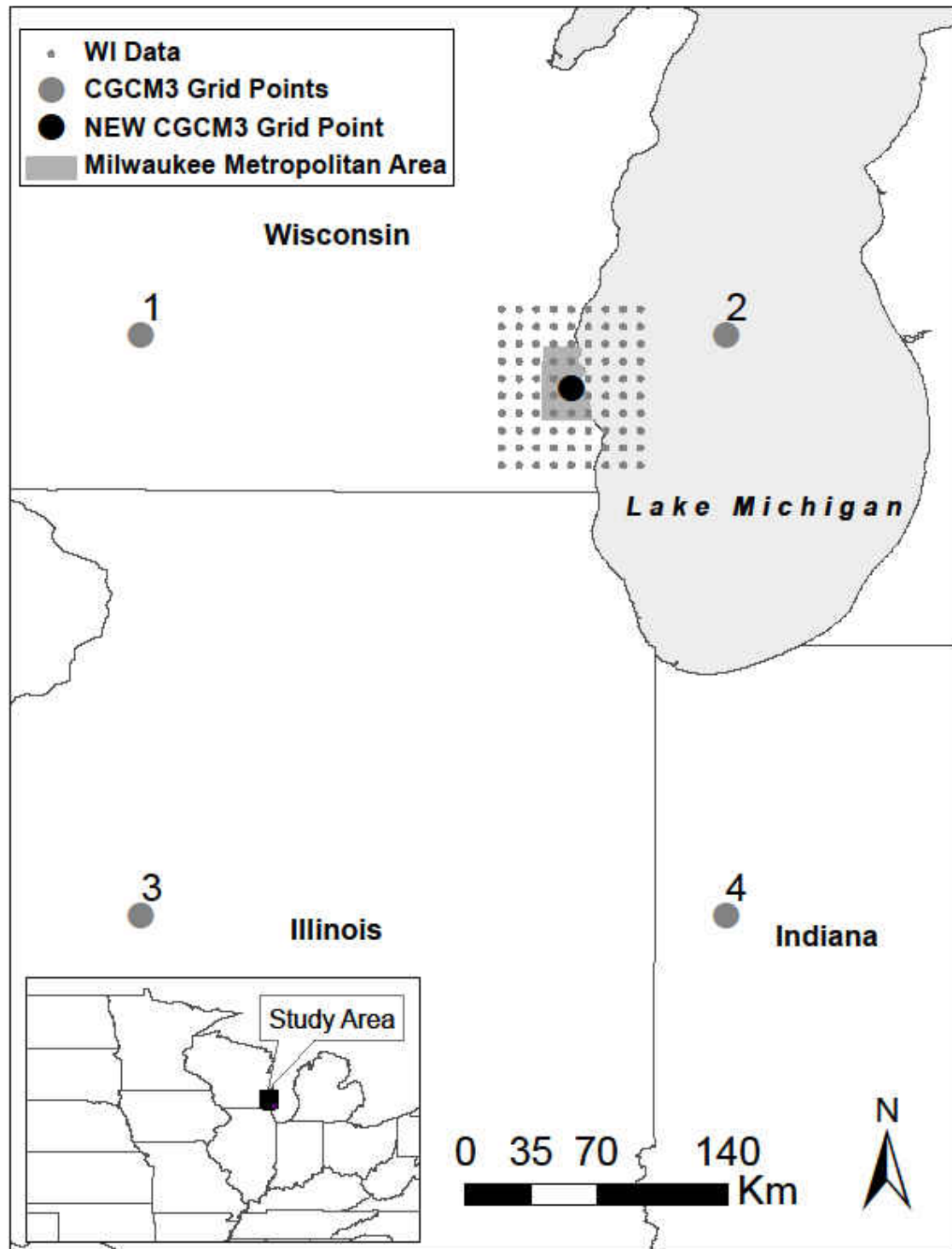
Fig. 1: Location of high-resolution gridded historical climatic dataset for Wisconsin grid points, the grid points from the CGCM3, and the created CGCM3 grid point, along with the administrative boundaries of the Milwaukee County

Chapter 4: Data

4.1   High-resolution Gridded Historical Climatic Dataset for Wisconsin

The daily precipitation from the high-resolution gridded historical climatic dataset for Wisconsin created by Serbin and Kucharik (2009) is used in this research. The gridded dataset is based on daily weather observations of maximum (T_{max}) and minimum temperatures (T_{min}) and total precipitation, from the NOAA cooperative (COOP) observer network stations, for 1950 – 2006 and interpolated to an 8 km (0.0833° Lat. x 0.0833° Long.) grid (Serbin and Kucharik 2009). Daily precipitation data from a total of 176 COOP observation stations, and 133 stations for T_{max} and T_{min}, within Wisconsin and a 70 km buffer were included in the interpolation process. Only stations with at least 53 years of data from 1950-2006 were included in the statistical interpolation (Serbin and Kucharik 2009).

The interpolation is based on the inverse distance weighting (IDW) spatial interpolation algorithm. Serbin and Kucharik (2009) explored other more complicated interpolation methods, e.g. kriging, thin plate splines, and determined that due to the high station density and low topographic complexity the IDW interpolation method resulted in comparable high quality results. Furthermore, these more complicated interpolation methods were rather restricted due to the smaller variance across data over flatter topography (Serbin and Kucharik 2009). Serbin and Kucharik (2009) found that the output accuracy of the predicted gridded precipitation is high, due to low mean daily total precipitation errors, and a realistic spatial distribution has been achieved. However, it is

likely that extreme precipitation events may have been smoothed over due to the nature of the interpolation method (Serbin and Kucharik 2009).

Daily precipitation data from 90 grid points were extracted, encompassing Metro Milwaukee and approximately a 24 km buffer around it. The study area is comprised of a rectangle of 9 latitudinal and 10 longitudinal grid points reaching from 42.62° - 43.37° latitude and 87.6° - 88.26° longitude. Furthermore, to gain a better insight into spatial differences within the study area, the 90 grid points were divided into 9 different groups: Northwest, North, Northeast, West, Metro, East, Southwest, South, and Southeast (Fig. 2). The border of each group and number of included grid points is based on the borders of Metro Milwaukee, and the land water border. Therefore, the number of grid points in each group varies from 6 to 14 points.
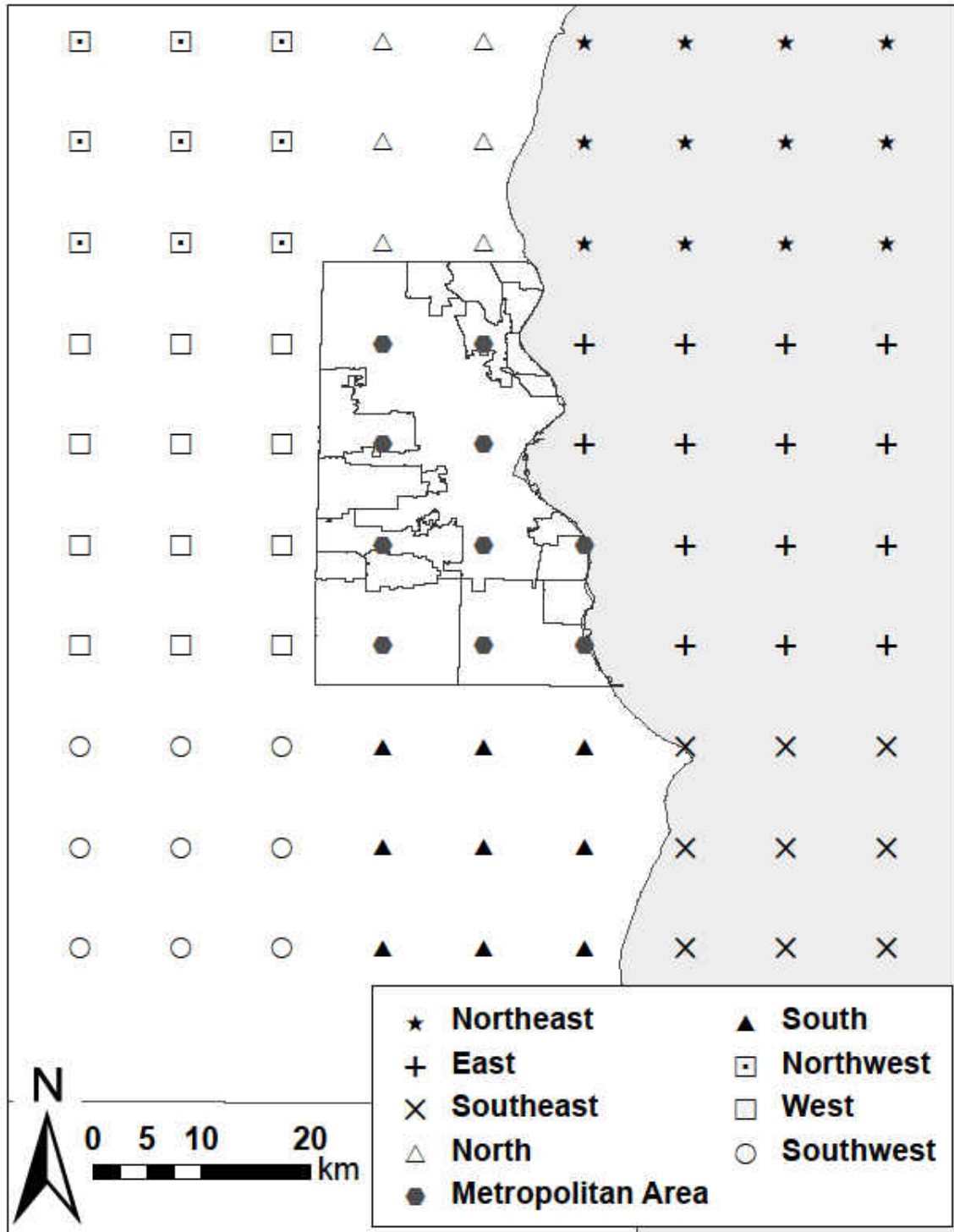
Fig. 2: Location of the grid points selected for each of the 9 groups from the high-resolution gridded historical climatic dataset for Wisconsin

4.2   Third Generation Coupled Global Climate Model (CGCM3)

The Canadian Centre for Climate Modeling and Analysis (CCCma) (http://www.ec.gc.ca/ccmac-cccma/) provides daily data for the Third Generation Coupled Global Climate Model (CGCM3), the latest developed version as used in the most recent IPCC assessment report (AR4). The CGCM3 is based on the ocean component that is used in the earlier Second Generation Coupled Global Climate Model, and an updated atmospheric component. The CCCma provides daily GCM data for several surface and atmospheric variables for the CGCM3 (http://www.cccma.ec.gc.ca/models/cgcm3.shtml) for two different resolutions: T63 and T47. The T63 has a horizontal resolution of 2.8° latitude by 2.8° longitude and a vertical resolution of 31 levels. The T47 is based on a 3.75° longitude/ latitude resolution with a vertical resolution of 31 levels.

Daily precipitation data was obtained for the CGCM3 climate for the 20th century (20CM3) experiments (1961-1990) and two future time periods, 2041-2070 (2050s) and 2071-2100 (2090s), for the IPCC Special Report on Emission Scenarios (SRES) A1B, A2, and B1 scenarios.

The daily precipitation data for four CGCM3 grid points (see table 1) within closest proximity to Metro Milwaukee were downloaded. As the closest CGCM3 grid point is approximately 66.7 km from the study area a new 'CGCM3' point in the center of the study area was created (Fig 1). The weighted distance from each of the selected CGCM3 grid points to the new created point is used to calculate the daily precipitation for the new point (see table 1). The daily precipitation for this new 'CGCM3' point is

calculated for the 20th century and each of the emission scenarios for the two future time periods.

Table 1: Geographic information of the selected CGCM3 grid points and the distance used to calculate the precipitation amount for the new CGCM3 grid point used for the downscaling process

Grid Point	Latitude (° N)	Longitude (° W)	Distance to new 'GCM' point (km)
1	43.2542	90	170.707
2	43.2542	87.1875	66.767
3	40.4636	90	330.114
4	40.4635	87.1875	288.421

Chapter 5: Methods

The delta method is used as the statistical downscaling algorithm to create high resolution precipitation projections for the future. To identify the trend two statistical tests are performed. First, the Mann-Kendall rank statistic method is applied to determine the significance of the trend, followed by the Sen's slope method to assess the magnitude of the observed change rates. The spatial analysis of the data is based on the inverse distance weighting interpolation algorithm. The inverse distance weighting function, as available in ArcGIS 10, is utilized for this study.

5.1   Delta Method

The standard approach for the delta method, also known as the change factor method or the perturbation method (Prudhomme, Reynard, and Crooks 2002), generates future prediction series based on General Circulation Model (GCM) outputs by quantifying the percentage differences of monthly mean precipitation between the reference period and the future (Olsson et al. 2009). The future downscaled precipitation is then calculated by superimposing the relative changes to the historical precipitation data (Sunyer, Madsen, and Ang 2012). The standard form of the delta method only accounts for differences in the respective mean and therefore, possible changes in range and variability of the data are not taken into consideration (Diaz-Nieto and Wilby 2005; Olsson et al. 2009).This limitation was addressed by modifying the equation for the delta method based on the method suggested by Leander and Buishand (2007). The observed historical daily precipitation amount P_{obs} is transformed to the future amount P_{fut} by using the following equation (2):

$$P^{fut} = \alpha(P_{obs})\beta \qquad\qquad (2)$$

where in the standard delta method, β is unity and α is the ratio of the mean monthly future precipitation to the mean monthly control precipitation, both based on GCM simulations. The control precipitation is most often based on the time period 1961-1990 which will also be used as the reference period in this study. For the modification of the method, the parameters α and β are based on the numerical optimization values and produce the mean and standard deviation (SD) of P_{fut}:

$$\bar{P}_{fut} = \bar{P}_{obs} \times \frac{\bar{P_f}}{\bar{P_c}} \qquad\qquad (3)$$

$$\sigma(P_{fut}) = \sigma(P_{obs}) \times \frac{\sigma(P_f)}{\sigma(P_c)} \qquad\qquad (4)$$

where P_c is the daily precipitation series from the control period GCM run and P_f is the daily precipitation series from the future GCM run. σ stands for the standard deviation and the over-bar denotes the average of the corresponding time period.

For this research, the MATLAB function (see appendix) based on that used in the study by Choi et al. (2009) was utilized. The control precipitation (P_c) for the 1961 – 1990 period, and the future precipitation (P_f) for 2041-2070 and 2071-2100 are based on the CGCM3. The historical observed daily precipitation was obtained from the high-resolution gridded historical climatic dataset for Wisconsin for the same time as the CGCM3 base period 1961-1990. According to Barrow (2000) the baseline period must coincide with the time period that was used to construct the climate change scenario. In other words, if the climate scenarios have been calculated in respect to the 1961-1990 time period it would be incorrect to apply these scenarios to a different time period. In order to determine the extent of future climate change, the selected time period should correspond to the baseline period used to generate the climate scenarios. For most of the

currently available climate scenarios 1961-1990 is defined as the baseline period. Based

on the historical dataset the future downscaled precipitation was obtained with the means

of the delta method (Fig.3).
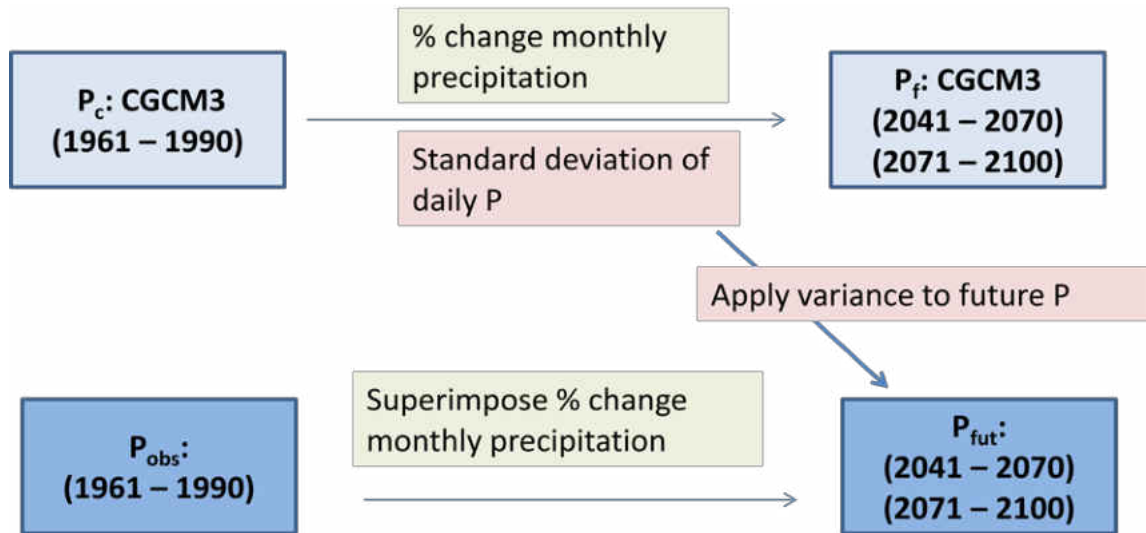
Fig. 3: Data and approach of the delta method used in this study

5.2 Mann-Kendall Rank Statistic Method

The Mann-Kendall (Mann 1945; Kendall 1975) test for trend was used to

investigate the temporal trend for the current time period. The non-parametric rank-based

test is very often used to test randomness against trend (Mitchell et al. 1966) and does not

assume any specific data distribution form, which makes it powerful and popular for

testing trends in hydrometeorological time series (Zhang et al. 2005; Toreti et al. 2009;

Zhang et al. 2009). For this research the procedure described by Manly (2009) was used

and calculated in the statistical program MATLAB based on a scripted function following

the given formula:

$$S = \sum_{i=2}^{n} \sum_{j=1}^{i-1} \text{sign}\,(x_i - x_j) \tag{5}$$

where for a series x_n the test statistic S is the sum of the signs of the differences between any two observations, and where sign(z) is 0 when z is zero, 1 when z is positive and -1 when z is negative.

If series of values in a random order, the expected value of S is zero and the variance VS is given as follows:

$$VS = n(n-1)(2n+5)/18 \tag{6}$$

Whether S is significantly different from zero can be tested by using the Z statistic, which is given as follows:

if $S > 0$

$$Z = \frac{S-1}{\sqrt{VS}}$$

else

$$Z = \frac{S+1}{\sqrt{VS}} \tag{7}$$

Z follows the standard normal distribution, and a positive Z value indicates a positive trend and a negative one indicates a negative trend in a two-sided test for trend. In this case the Z values were converted to probabilities of observing larger absolute Z values. In order to show the significance of a trend the p value was calculated as follows:

$$p = 2 * \Phi(-|Z|) \tag{8}$$

where Φ is the normal cumulative distribution function.

If $p \leq 0.05$ the temporal trend is significant, is $p > 0.05$ the trend is insignificant.

5.3   Sen's slope

The trend of precipitation variables was calculated based on the Sen's slope test. The Sen's slope test is a non-parametric test of trend and calculates the slope based on a linear model to estimate the trend (Sen 1968).The trend of a time series can be estimated based on the slope of the data. The Sen's slope estimator calculates the slope (S) of the data x as follows:

$$S = \text{median}(y) \tag{9}$$

$$y = \left(\frac{xi-xj}{i-j}\right) \qquad i = 1,2,3….N \text{ and } i < j \tag{10}$$

If there are n values of x in the time series we get as many as N = n(n-1)/2. The slope of the time series is given in proportional values based on the size of the data values.

5.4   Inverse Distance Weighting (IDW)

The interpolation of precipitation variables is based on the inverse distance weighting (IDW) algorithm available in ArcGIS 10. IDW is based on the assumption that points closer to each other are more alike than those further apart. The values surrounding the location of interest will be used to calculate the value of the location of interest and can be described as a distance reverse function of the prediction location from neighboring points (Johnston et al. 2001). Thus, this method is based on the idea that each existing point has a local influence that diminishes with distance. The IDW algorithm uses a linear-weighted combination of sample points within a defined neighborhood (Johnston et al. 2001).

The IDW formula is as follows (Johnston et al. 2001):

$$Z_x = \frac{\sum_{i=1}^{N} Z_i * d_{ix}^{-n}}{\sum_{i=1}^{N} d_{ix}^{-n}} \tag{11}$$

where:

Z_o = the estimation value for an unknown point at location x
Z_i = the observed value at the known point i
d_{io} = the distance from the known point i to the unknown point x
n = power parameter which controls the significance of the surrounding points

The main factor affecting the accuracy of the IDW algorithm is the selected power parameter (n). The higher the power predictor value, the more emphasis is placed on closer locations. A smaller value of the power predictor creates a smoother surface and a higher weight is placed on more distant stations (Johnston et al. 2001). According to the literature, a power value of 2, known as the inverse square of the distance, is commonly used with IDW and is the default setting in ESRI's ArcGIS 10 (Nalder and Wein 1998; Jarvis and Stuart 2001).

5.5   Representative Precipitation

In order to analyze the average precipitation for the entire study area and furthermore to address the variability of precipitation across the study area, a variable representing the average precipitation was calculated. A similar approach as that used by Schlünzen et al. (2010) has been adopted in this study. Schlünzen et al. (2010) averaged the daily precipitation measurements if the daily precipitation was at least 1 mm at a minimum of 2 of the 9 selected sites in order to create a measure for the area representative precipitation. The difference between the area representative precipitation and the precipitation at the selected sites is used to determine the urban induced precipitation (Schlünzen et al. 2010).

In this research, the variable expressing the representative precipitation is calculated as the median of the 90 grid points. All precipitation values are included in the calculation of representative precipitation. This was decided because, generally when the precipitation was 0 mm at one grid point it was the same for the whole study area. The representative precipitation (RP) is used to analyze the differences in precipitation within the study area by comparing the RP to the precipitation value of the individual station.

Chapter 6: Decadal Changes in Precipitation

6.1 Statistical Overview

Summary statistics for precipitation indices are presented in Table 2. The mean, median, and range in annual representative precipitation for the high-resolution gridded historical climatic dataset for Wisconsin for the period 1950 to 2006, and the CGCM3 data for 1961-1990 are presented in Table 2.   The annual 95th percentile of daily precipitation for both datasets is derived by calculating the 95th percentile of daily precipitation of more than 1mm for each calendar year (February 29th excluded).   The annual 95th percentile of daily precipitation is referred to as 95th percentile precipitation from here on. The representative precipitation of the 95th percentile precipitation is represented in table 2.

The mean representative precipitation results in 831 mm and the median in 848 mm for the historical climatic dataset. The averaged precipitation for the baseline period of the CGCM3 data results in a mean of 927 mm and a median of 906 mm. The averaged annual precipitation based on the CGCM3 data is overestimated in comparison to the observational data. The minimum and maximum annual precipitation for the historical climatic data of 547 mm and 1086 mm, is much lower than that of the CGCM3 data of 707 mm and 1180 mm.

The mean and median of the 95th percentile for the observational data with 24mm and 23mm respectively is higher than the mean and median for the CGCM3 with 17 mm. The maximum 95th percentile precipitation is higher for the observational data with a maximum of 31 mm and a minimum of 20 mm. The 95th percentile precipitation for the CGCM3 data rages from 11 mm to 23mm. The standard deviation for both the annual as

well as the 95th percentile are very close, which leads to the assumption that the variability between the two data sets is similar.

Table 2: Summary statistics for precipitation from the historical climatic WI dataset and the CGCM3 data

	Annual RP of P_{obs} 1950-2006	Annual CGCM3 1961-1990	95th percentile RP of P_{obs} 1950-2006	95th percentile CGCM3 1961-1990
Mean	831 mm	927 mm	24 mm	17 mm
Median	848 mm	906 mm	23 mm	17 mm
SD	126 mm	128 mm	2 mm	3 mm
Minimum	547 mm	707 mm	20 mm	11 mm
Maximum	1086 mm	1180 mm	31 mm	23 mm

6.2   Annual Precipitation

The mean annual total precipitation for 1950 – 2006 shows a large spatial variation with a range of 94 mm (Fig. 4). The highest precipitation (889 mm) can be found within the southeastern regions of the study area. The northern part of the study area is the driest with a low of 795 mm per year (Fig. 4) with a latitudinal decreasing pattern.
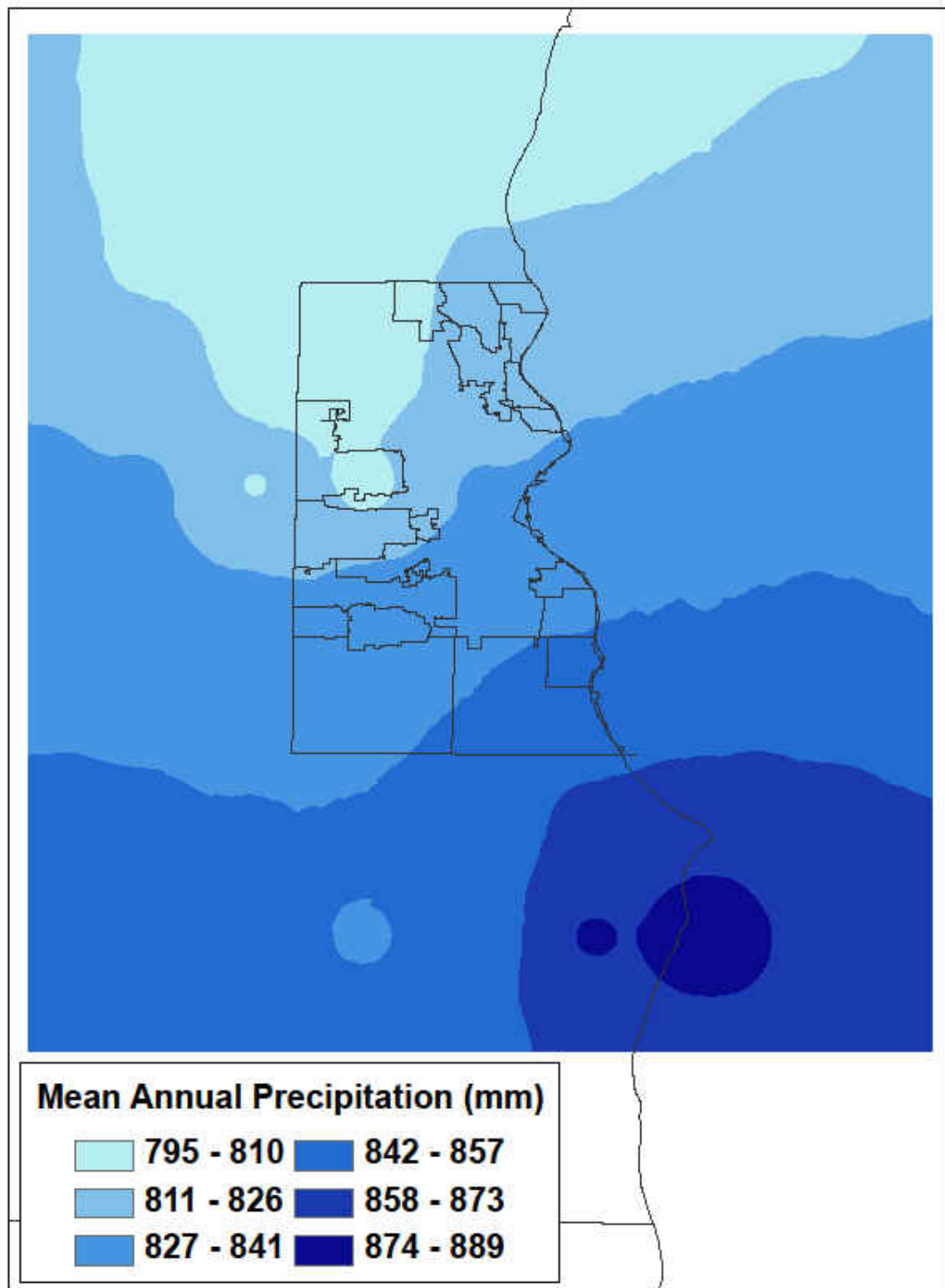
Fig. 4: Mean annual precipitation (mm) 1950 – 2006

Figure 5a displays the temporal variation in annual precipitation for the time period 1950 to 2006. The median precipitation amount of each year is indicated by the red line of each 'box'. The boxplot shows that the temporal variation of annual precipitation is very diverse and does not reveal any obvious trend. Figure 5b shows the annual RP subtracted from the total annual precipitation at each station. Averaged over the time period from 1950 to 2006, a large spatial variation in annual precipitation across the study area is presented. The spatial variation varies from year to year, stronger in some years and much less in others.
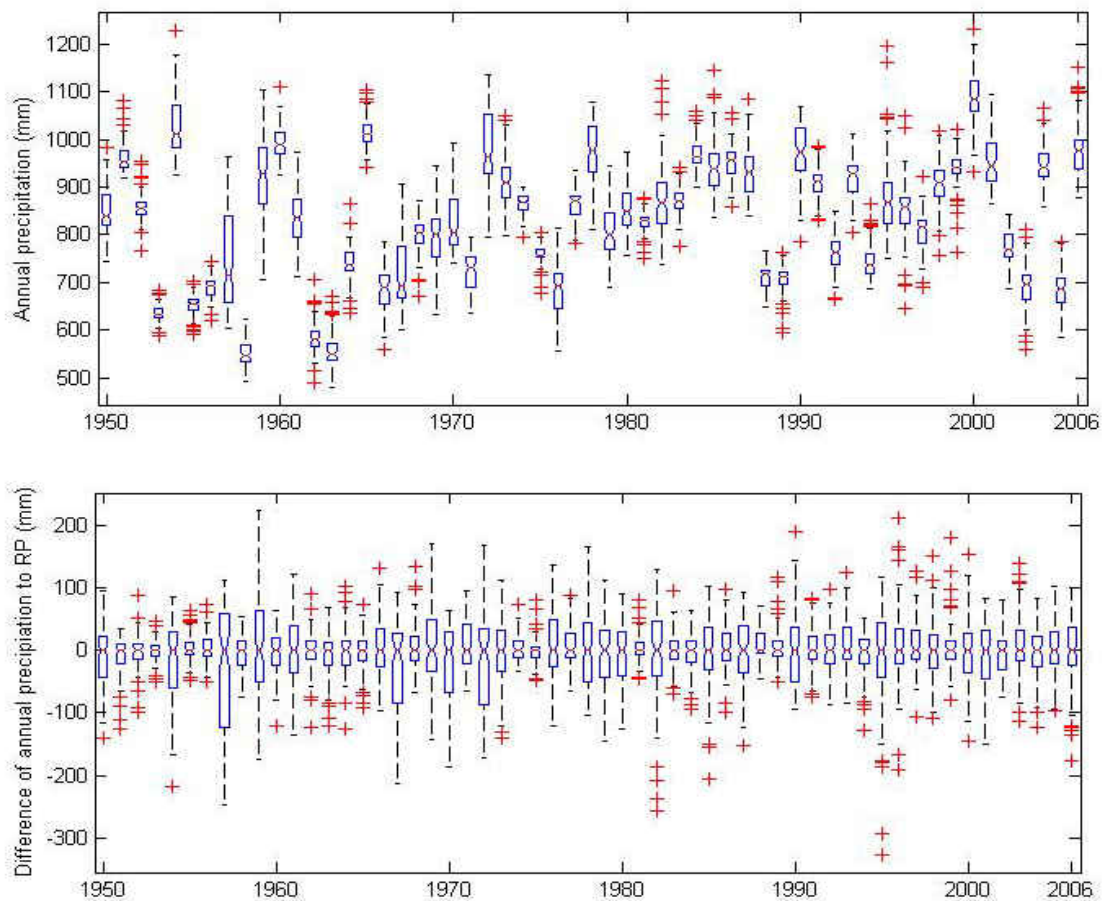
Fig. 5: (top) Annual precipitation 1950-2006; (bottom) Difference of RP and stations based on annual precipitation 1950 – 2006

Figure 6 displays the regional differences within the study area, the difference between the median of each group and the RP of the whole study area. The northern regions of the study area (groups: Northwest, North, Northeast) receive less annual precipitation than the average across the whole study area. The northern region, right above Metro Milwaukee, shows the largest deviation in annual precipitation of -20 mm compared to the average of the study area, and receives the least amount of precipitation. The average precipitation in the southern regions (groups: Southwest, South, Southeast) is higher compared to the average precipitation across the whole study area. This indicates that the southern regions receive on average more rain. The highest precipitation within the southern area occurs in the southeastern region over Lake Michigan decreasing towards the west. Metro Milwaukee and the area to the west show a slightly lower precipitation (ca. 3 mm) than the average across the study area. The area east of Metro Milwaukee receives slightly more precipitation (ca. 6 mm) than the average of the whole study area. The regional analysis of precipitation differences within the study area indicates the highest precipitation in the southern regions, especially in the southeastern areas (Fig 6). A decreasing trend with latitude can be observed with the lowest precipitation in the northwestern areas (Fig 6). Metro Milwaukee shows only slightly lower average annual precipitation compared to the whole study area, but is overall very close to the median of the study area.
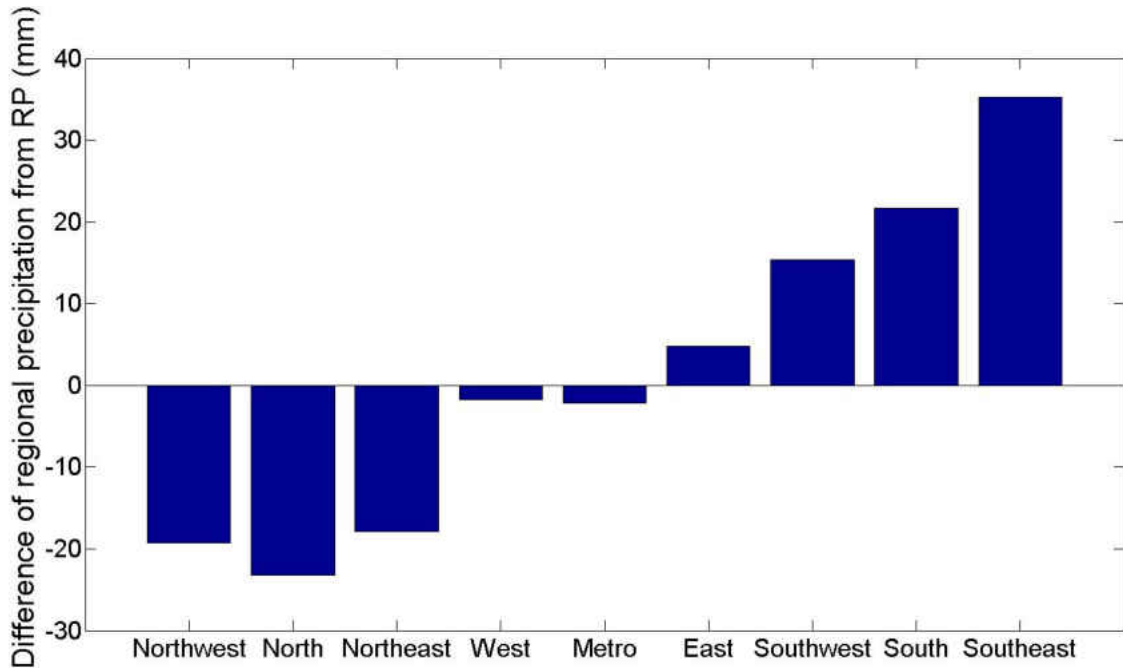
Fig. 6: Difference of regional precipitation from RP for 1950 - 2006

Figure 7 shows the slope and significance of trend for total annual precipitation at the 95 percent confidence interval. The highest increasing trends can be found northwest of Metro Milwaukee, the southern parts of Metro Milwaukee and the northern and central parts over Lake Michigan (Fig. 7a). The grid-points with the strongest increasing trends are of significance. Forty-five grid points show a significant trend and are located in the northern and eastern parts of the study area and Metro Milwaukee (Fig. 7b). Only two grid points, in the far southwest corner show a negative trend. However, these trends are not significant.
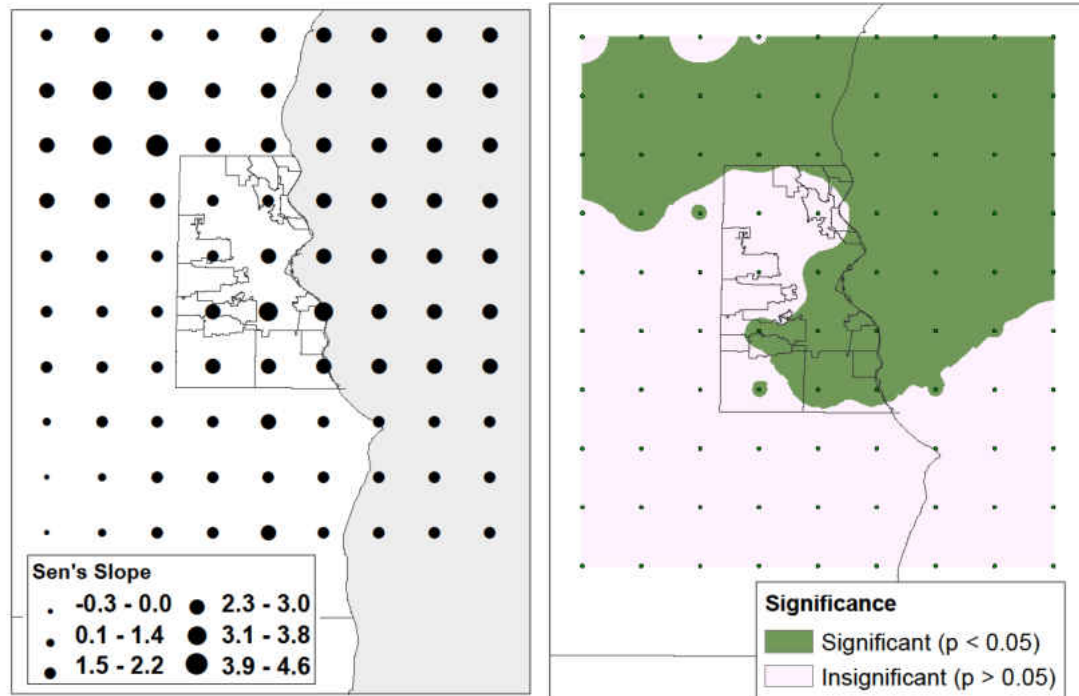
Fig. 7: Results from the (left) Sen's slope test for trend of annual precipitation, (right) Mann-Kendall test significance of annual precipitation

6.3 Monthly Precipitation

The mean monthly precipitation based on the high resolution observational dataset from 1950 to 2006 shows a distinguished seasonal pattern (Fig. 8). The driest time of the year is during winter (December, January, February), and the summer season (June, July, August) experiences the wettest months. The mean monthly precipitation shows a large spatial variation across the study area. The highest average monthly precipitation is observed in July (96 mm) and the lowest average monthly precipitation (32 mm) in February.
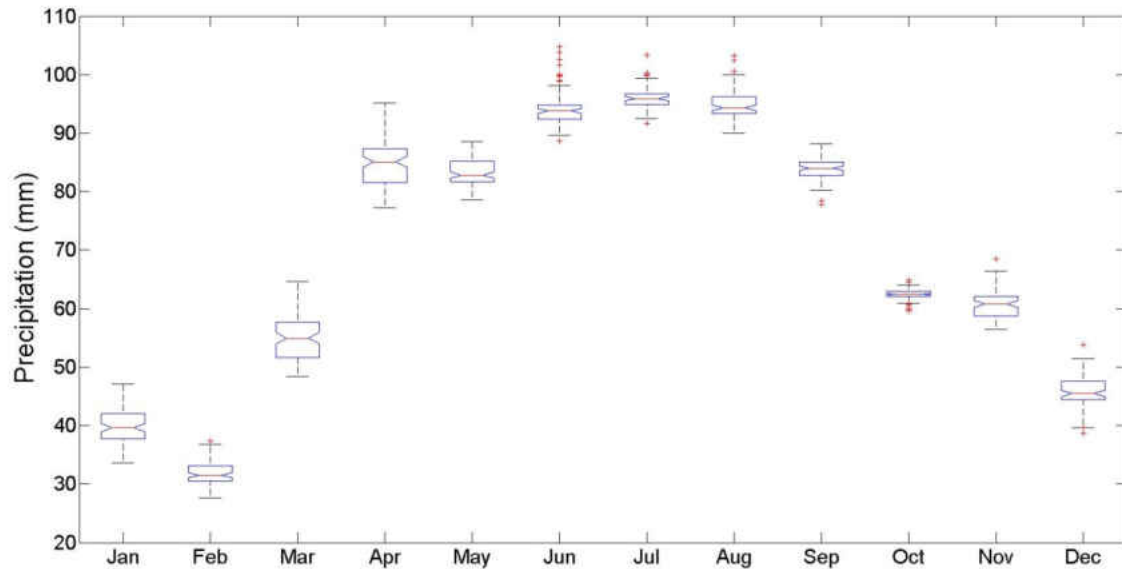
Fig. 8: Mean monthly precipitation for 1950 – 2006

The spatial variation of mean monthly observational precipitation averaged over the time period from 1950 to 2006 is shown in Figure 9a and 9b. The mean monthly precipitation amount from each grid point was interpolated using the IDW algorithm. Each month's results were classified in six groups based on equal intervals. In Figure 9a the spatial variation of mean monthly precipitation for the months January through June are displayed, the months July though December are shown in Figure 9b. A unique spatial pattern for each month can be seen. Focusing on Metro Milwaukee, the winter months (December – January) show high precipitation centers over the metropolitan area spreading towards the southeast, and the driest areas are found in the northwestern regions of the study area. In spring (March – May) the northwestern part of the study area is driest, and the southeastern region the wettest. In summer the driest areas are moving towards the northeastern parts and the wettest areas are found in the southwest (June) and west (July, August). A distinguished center of low precipitation over Metro Milwaukee can be observed in May, July (very small), September, October, and November.

January
- 33.7 - 35.9
- 36 - 38.1
- 38.2 - 40.4
- 40.5 - 42.6
- 42.7 - 44.9
- 45 - 47.1

February
- 27.6 - 29.2
- 29.3 - 30.9
- 31 - 32.5
- 32.6 - 34.1
- 34.2 - 35.7
- 35.8 - 37.4

March
- 48.4 - 51.1
- 51.2 - 53.8
- 53.9 - 56.5
- 56.6 - 59.2
- 59.3 - 61.9
- 62 - 64.6

April
- 77.3 - 80.3
- 80.4 - 83.2
- 83.3 - 86.2
- 86.3 - 89.2
- 89.3 - 92.2
- 92.3 - 95.2

May
- 78.5 - 80.2
- 80.3 - 81.9
- 82 - 83.5
- 83.6 - 85.2
- 85.3 - 86.9
- 87 - 88.6

June
- 88.7 - 91.4
- 91.5 - 94
- 94.1 - 96.7
- 96.8 - 99.4
- 99.5 - 102.1
- 102.2 - 104.8
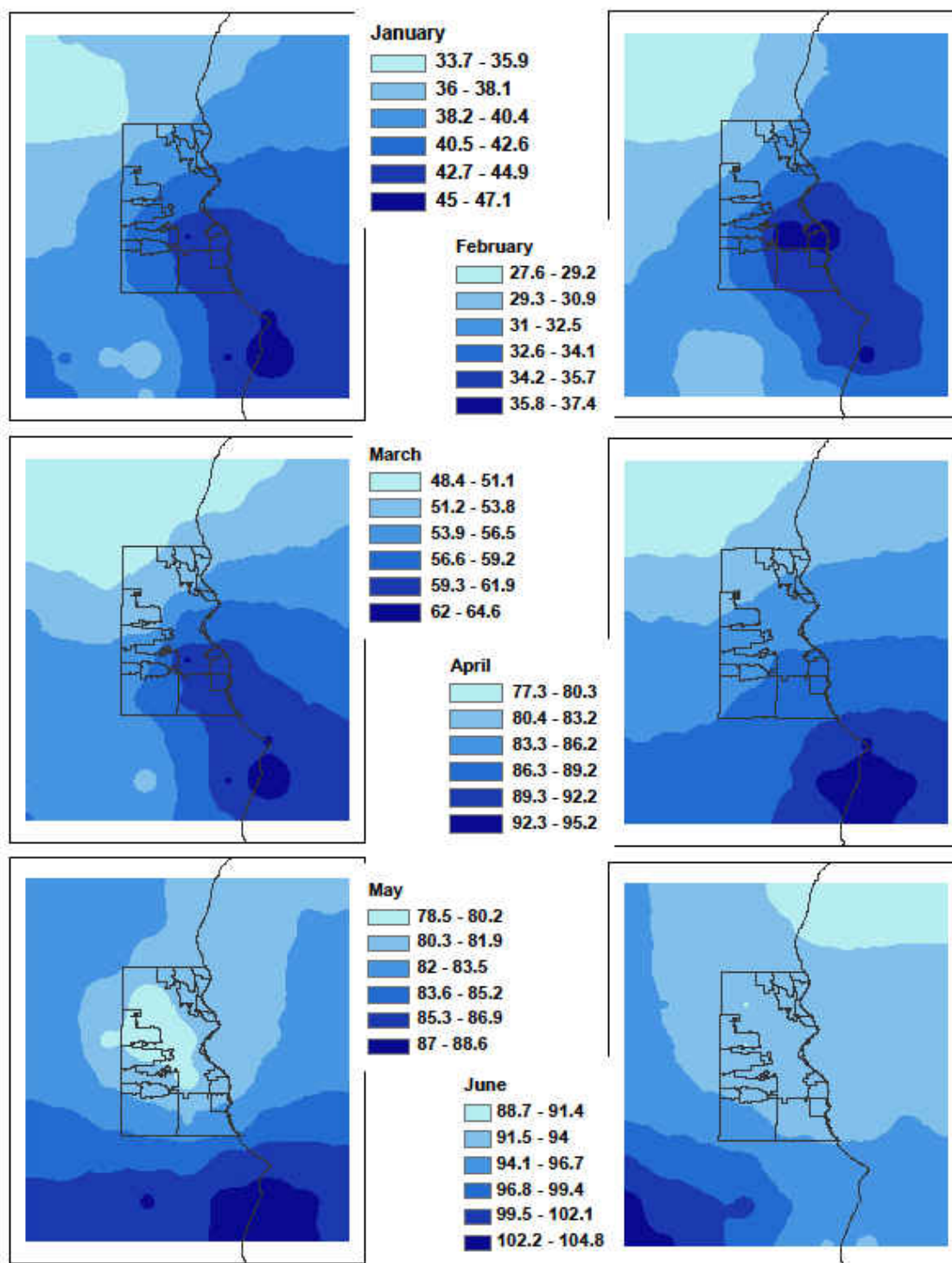
Fig 9a: Spatial variation of mean monthly precipitation (mm) for 1950 - 2006 for January to June
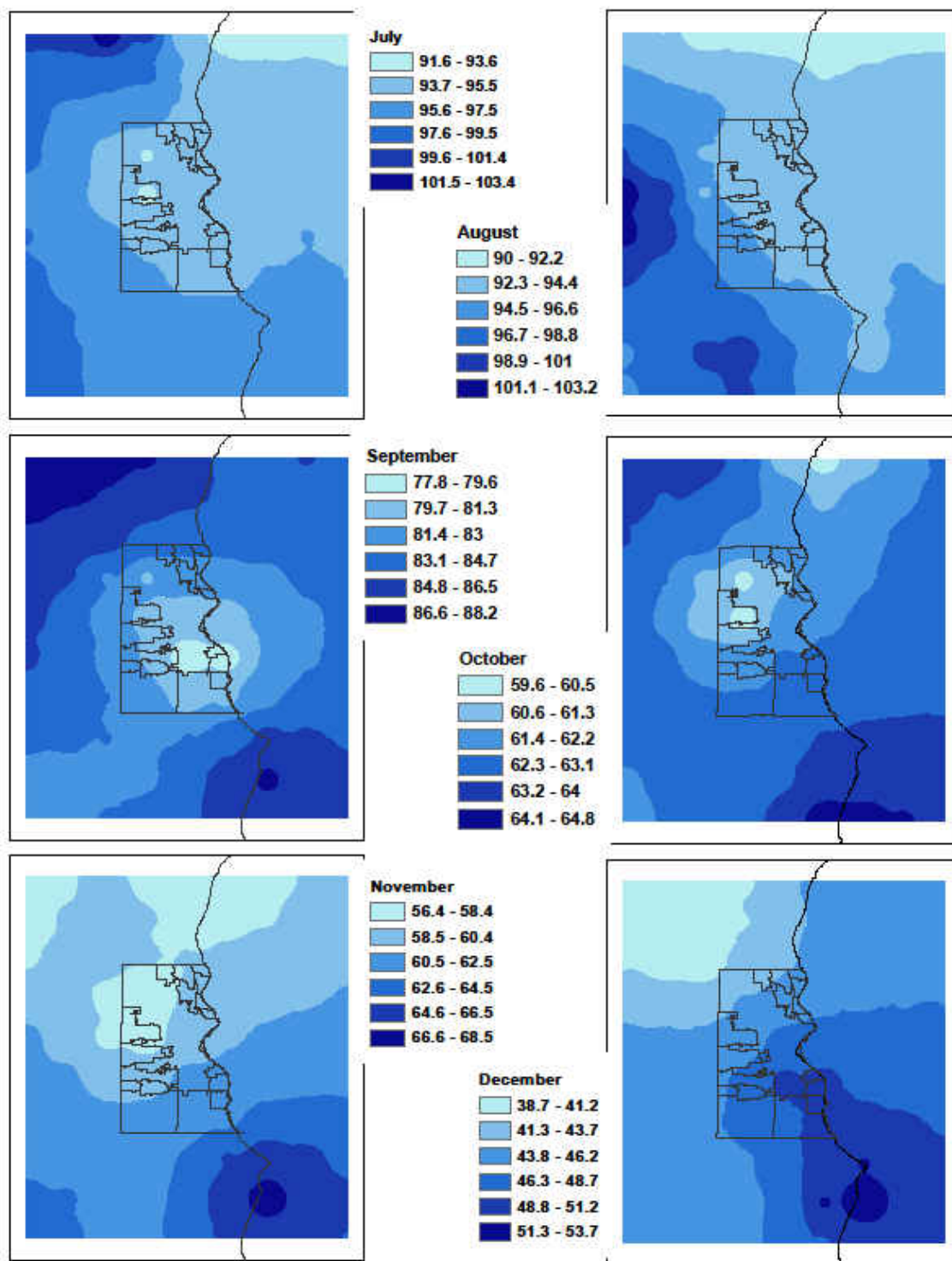
Fig 9b: Spatial variation of mean monthly precipitation (mm) for 1950 - 2006 for July to December

6.4   Extreme Precipitation

The spatial variation of the 95th percentile precipitation is homogenous, and also varies from year to year but not as drastically as the annual precipitation sum. The spatial variation of the 95th percentile precipitation ranges from approximately 12mm to 15 mm (Fig. 10). The highest precipitation occurs in the southeastern parts of the study area and the lowest to the northeast and east over Lake Michigan.
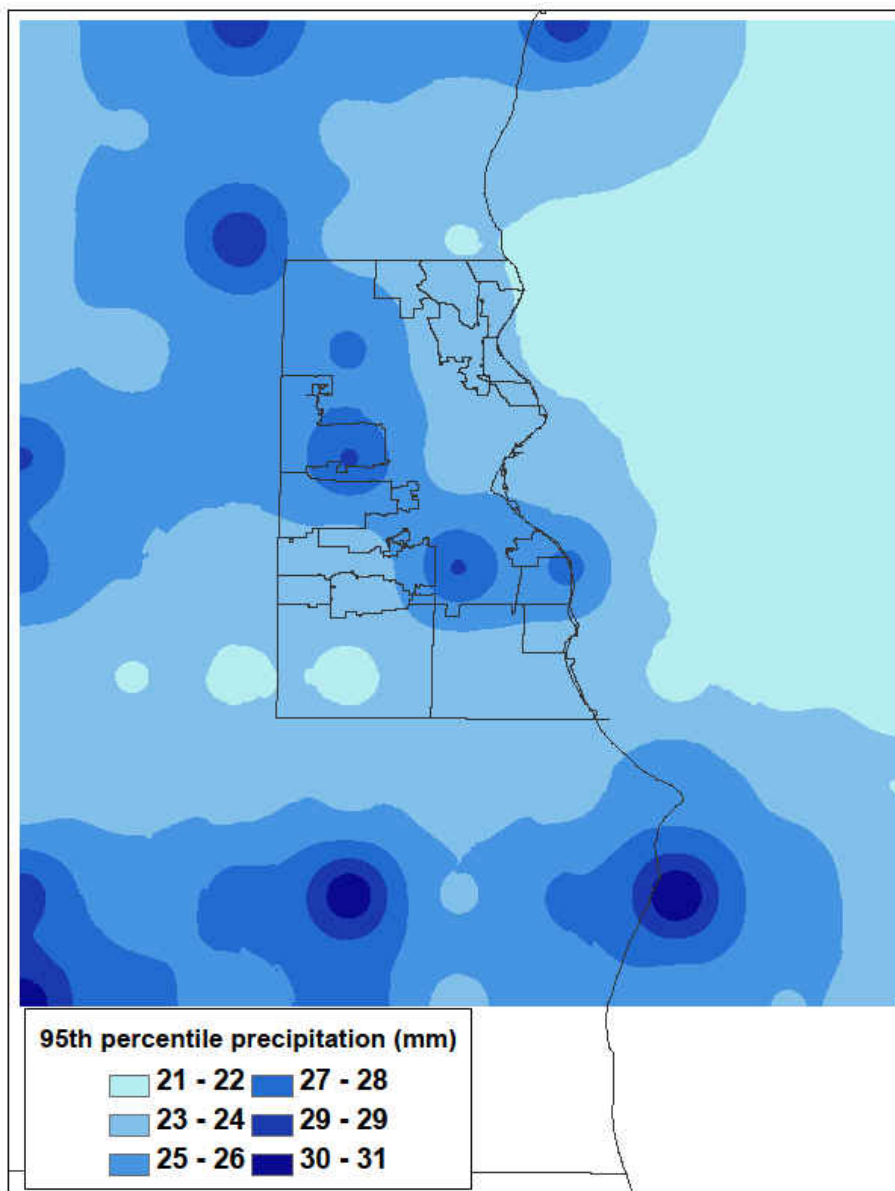
Fig. 10: Spatial variation of 95th percentile precipitation for 1950 - 2006

The Sen's slope analysis and Mann-Kendall test of trend of the 95th percentile precipitation is presented in Figure 11. The highest increases in the 95th percentile precipitation are observed within the northeastern and western parts of the study area. The southern and eastern areas show a negative trend. Overall the 95th percentile of annual precipitation trend shows a high variability. Only a few isolated grid points at the northern border of the study area and one southeast of Metro Milwaukee show a significant trend.
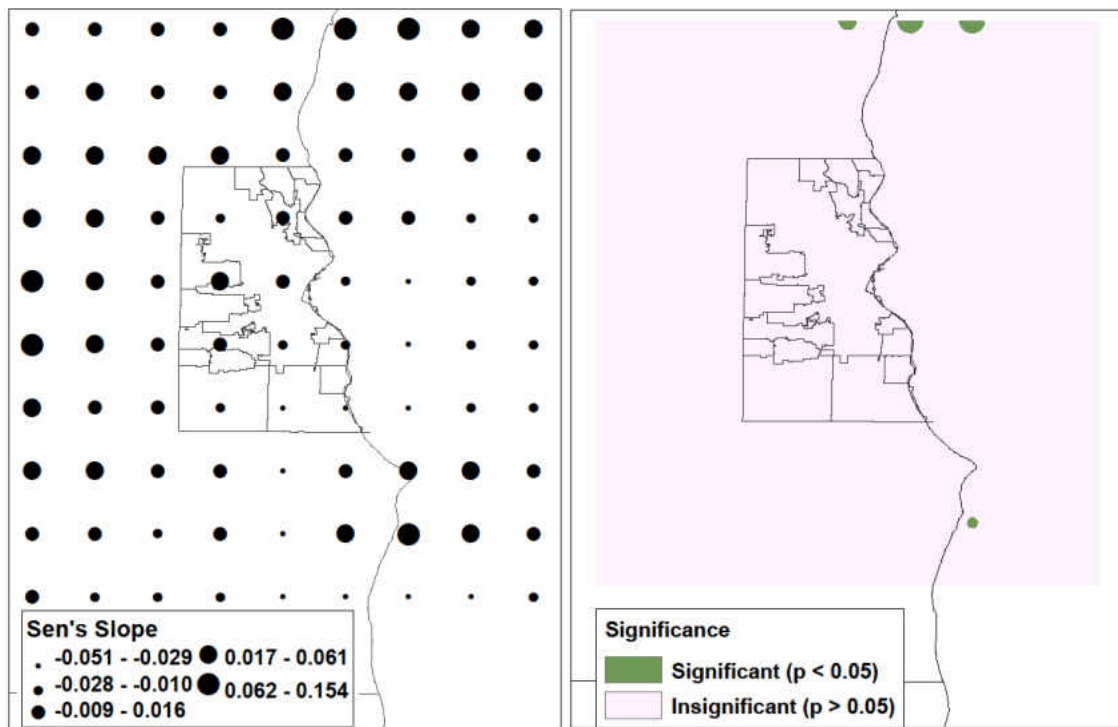
Fig. 11: Results from the (left) Sen's slope test for trend of 95th percentile precipitation, (right) Mann-Kendall test significance of 95th percentile precipitation

Chapter 7: Projected Changes in Precipitation

7.1   Statistical Overview

The summary statistics for the projected precipitation characteristics from the delta method downscaling results are presented in Table 3 and 4. The representative precipitation averages, standard deviation, and range are calculated for the 2050s and 2080s for all three emission scenarios A1B, A2, and B1. For all three emission scenarios the mean annual precipitation is predicted to increase in the future. Considerable variations in mean annual precipitation are projected for the 2050s and 2080s. For the 2050s the highest mean annual precipitation of 945 mm is predicted for the A1B scenario. The precipitation for the A2 and B1 scenario is predicted to be much lower with 902 mm and 878 mm respectively. The annual precipitation varies considerably over the study area with a range of 1225 mm for the A1B scenario, 1173 for the A2, and the lowest range of 1127 mm for the B1 scenario. The annual precipitation for the 2080s for the A2 and B1 scenarios are predicted to be higher than the 2050s with 926 mm and 904 mm. For the A1B scenario the mean annual precipitation is predicted to be lower than in the 2050s with 927 mm. The range also increases for the A2 and B1 scenario, whereas the difference for the A1B scenario is predicted to be slightly less (Table 3).

Table 3: Summary statistics for annual representative precipitation from the downscaled results

	2050s A1B	2050s A2	2050s B1	2080s A1B	2080s A2	2080s B1
Mean	945 mm	902 mm	878 mm	927 mm	926 mm	904 mm
Median	935 mm	893 mm	872 mm	915 mm	915 mm	897 mm
Standard deviation	154 mm	146 mm	141 mm	144 mm	152 mm	145 mm
Minimum	586 mm	562 mm	535 mm	587 mm	571 mm	562mm
Maximum	1225 mm	1173 mm	1127 mm	1211 mm	1210 mm	1177 mm

The projected averages, standard deviation, and range from the downscaled results of the representative 95th percentile precipitation are shown in Table 4. The mean and median precipitation for the A1B, A2, and B1 emission scenarios for the 2050s are within 1 mm to the 95th percentile precipitation amounts projected for the 2080s. The standard deviation of 3 mm is very small and the same for all three emission scenarios in both time periods. The spatial variation is very homogenous over the region and very similar for the 2050s and 2080s for all three emission scenarios.

Table 4: Summary statistics for the 95th percentile precipitation from the downscaled results

	2050s A1B	2050s A2	2050s B1	2080s A1B	2080s A2	2080s B1
Mean	30 mm	30 mm	30 mm	29 mm	30 mm	30 mm
Median	29 mm	29 mm	29 mm	29 mm	29 mm	30 mm
Standard deviation	3 mm	3 mm	3 mm	3 mm	3 mm	3 mm
Minimum	26 mm	26 mm	26 mm	26 mm	26 mm	26 mm
maximum	40 mm	40 mm	39 mm	38 mm	41 mm	41 mm

7.2 Annual Precipitation

Figure 12 shows the changes in mean annual representative precipitation from the observational data for 1950-2006 to the future downscaled scenarios for the 2050s and 2080s for all three emission scenarios. The precipitation is predicted to increase by almost 14% from the current time period to the 2050s and by ~ 12% by the 2080s in the A1B emission scenario. The percentage change in mean annual precipitation based on the A2 and B1 emission scenarios are predicted to change by ~ 8% and ~ 6% by the 2050s and by approximately ~ 12% and 9% by the 2080s. The two-sample t-test, as available in MATLAB as the 'ttest2' function, was used to analyze the significance of these changes in mean annual precipitation. The changes for all but the results of the B1 scenario for the 2050s were of significance at the 95 percent confidence interval.
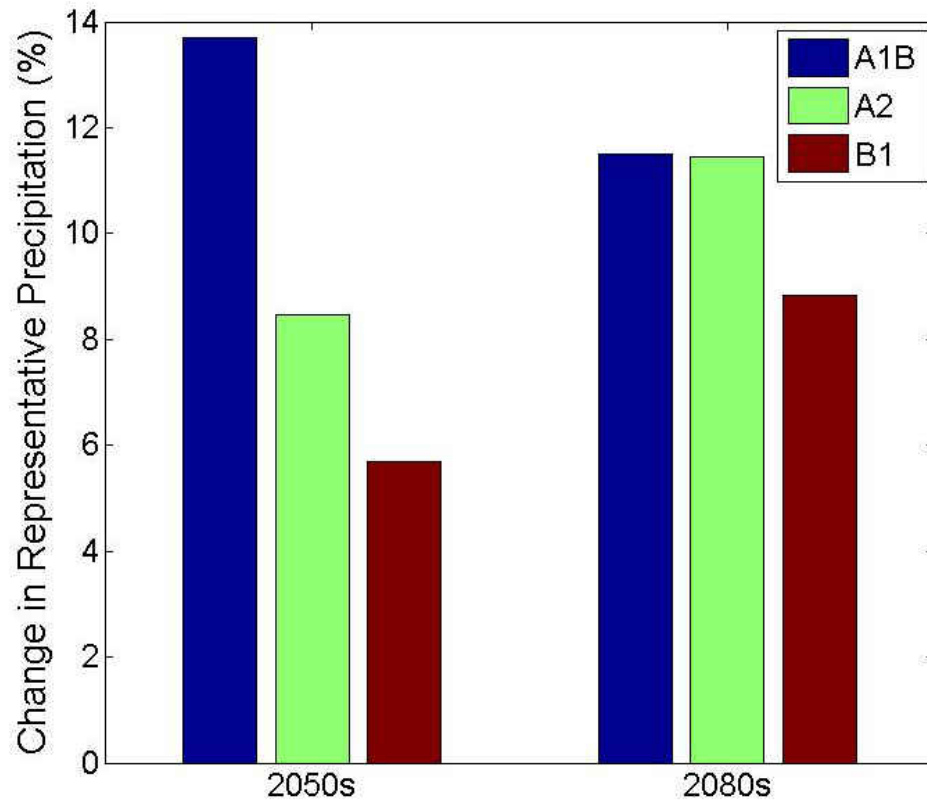
Fig. 12: Changes in mean annual representative precipitation from 1950-2006 to the 2050s and the 2080s

The spatial variation of annual precipitation for the 2050's is very heterogeneous across the study area. The spatial pattern of annual mean precipitation for the 2050's is very similar for all three future scenarios, with the highest precipitation predicted in the southeastern areas and the lowest precipitation in the southwestern region (Fig. 13). For the 2050s, the mean annual precipitation amount for the A1B emission scenarios ranges from the lowest precipitation of 893 mm to the highest precipitation of ca. 1003 mm (Fig. 13). Even though the spatial variation of precipitation is very similar, the mean annual precipitation for the A2 and B1 emission scenarios is lower, ranging from 850 mm - 960 mm and from 827 mm - 935 mm respectively (Fig. 13). The spatial pattern of annual precipitation scenarios for the 2080s is very similar to the pattern predicted for the 2050s, (Fig. 13) with the highest precipitation in the southeastern corner of the study area and

the lowest precipitation in the northwestern part of the study area. The overall precipitation amount is higher for the 2080s than for the 2050s (Fig. 13), with the exception of the downscaling results based on the A1B emission scenario (Fig. 13). In this case, the time period 2041-2070 experiences more precipitation (893-1003 mm) than the 2080s (Fig. 13) with the lowest precipitation of ca. 873 mm and the highest precipitation of 987 mm. The results based on the A2 and B1 emission scenarios receive comparably less precipitation than the A1B emission scenario based results. This difference is much stronger for the 2050s than the 2080s. The mean annual precipitation for the A2 and B1 emission scenario range from 869 mm - 991 mm and 853 mm - 962 mm respectively.

A1B 2050s
- 894 - 912
- 913 - 930
- 931 - 948
- 949 - 966
- 967 - 985
- 986 - 1,003

A1B 2080s
- 873 - 892
- 893 - 911
- 912 - 930
- 931 - 949
- 950 - 968
- 969 - 987

A2 2050s
- 851 - 869
- 870 - 887
- 888 - 905
- 906 - 923
- 924 - 941
- 942 - 959

A2 2080s
- 869 - 889
- 890 - 909
- 910 - 930
- 931 - 950
- 951 - 970
- 971 - 990

B1 2050s
- 828 - 845
- 846 - 863
- 864 - 881
- 882 - 899
- 900 - 917
- 918 - 935

B1 2080s
- 853 - 871
- 872 - 889
- 890 - 908
- 909 - 926
- 927 - 944
- 945 - 962
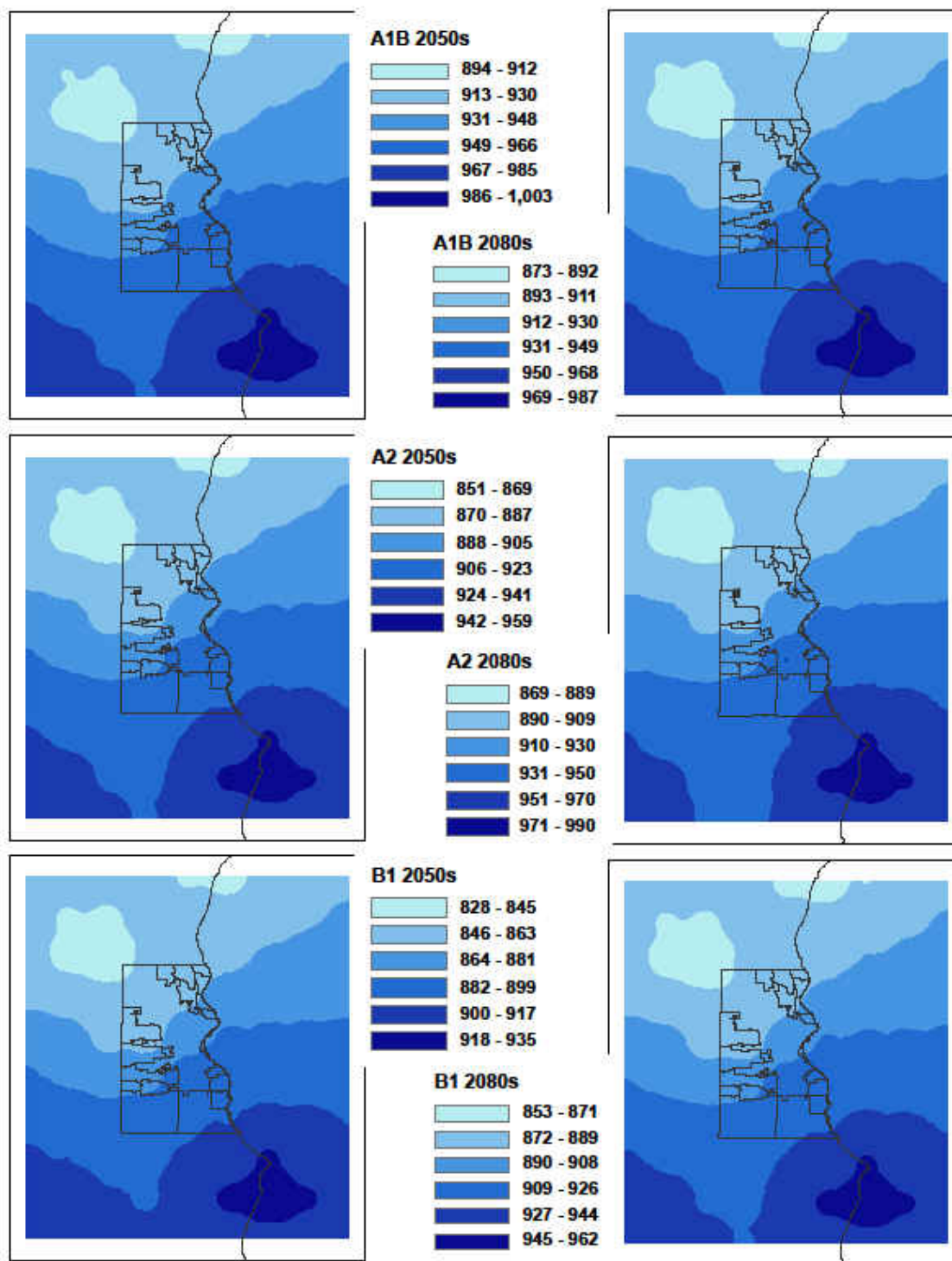
Fig. 13: Spatial variation of mean annual precipitation (mm) for the A1B, A2, and B1 emission scenario for the 2050s and the 2080s

In Figure 14 the projected spatial changes in mean annual precipitation for the 2050s and the 2080s have been mapped. The largest changes in mean annual precipitation from the current time period (1950-2006) to the 2050s, of approximately 14%, are predicted to occur in the southwestern regions, the far northwestern regions, and a small circle in the middle of Metro Milwaukee. The lowest changes occur northwest (ca. 11%) and southeast (ca. 12%) of Metro Milwaukee. The spatial changes from the current time period to the 2080s (A1B scenario) are very similar to that of the 2050s. The highest precipitation of approximately 12 mm is predicted for the southwestern part of the study area as well as in the central area of Metro Milwaukee. The lowest annual precipitation changes of ca. 8% are predicted to occur southwest of Metro Milwaukee. The predicted spatial annual precipitation changes for the 2050s and 2080s for the A2 and B1 emission scenarios are very similar to the A1B scenario only with lower percentage changes.
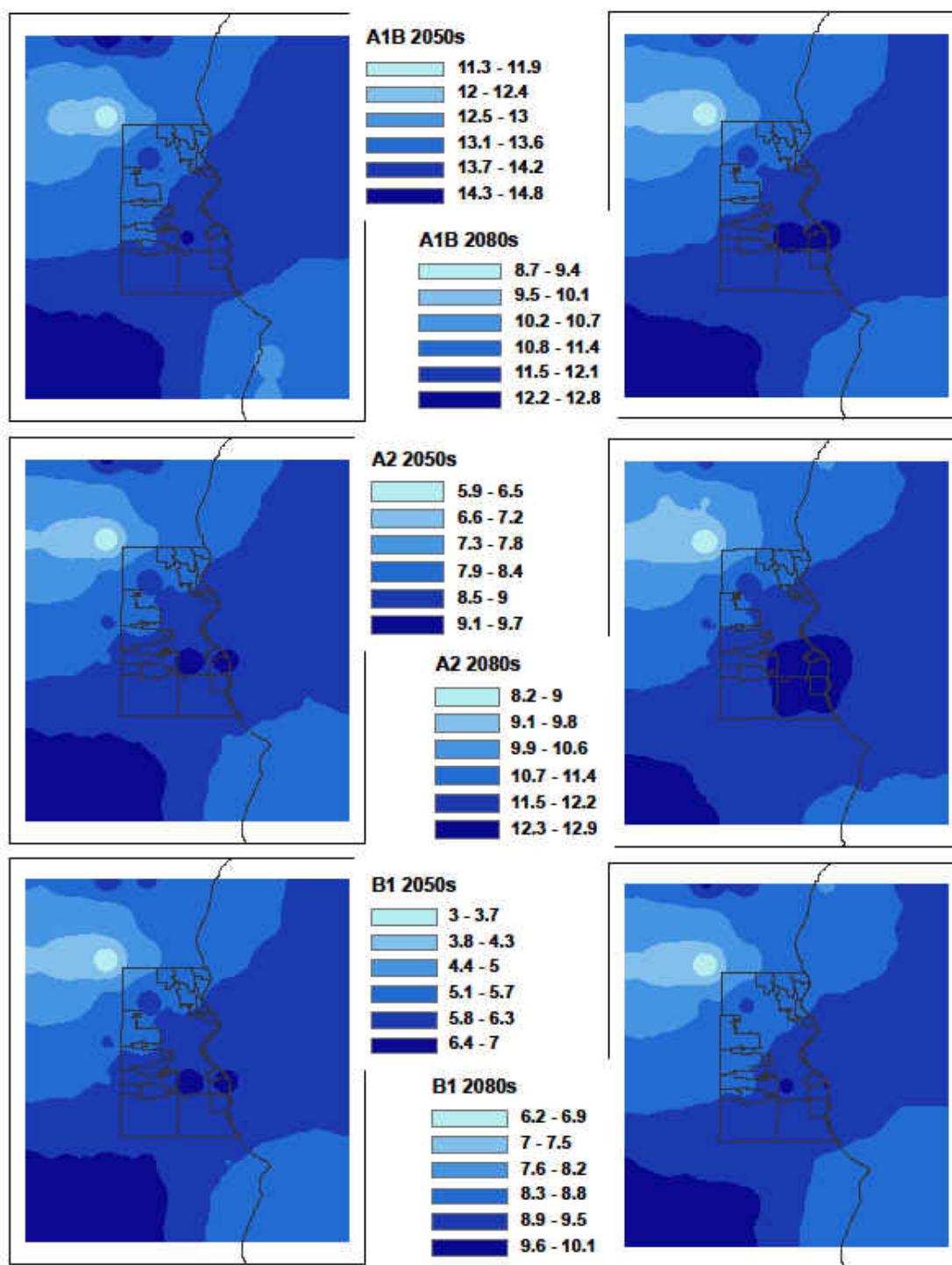
Fig. 14: Projected spatial changes in mean annual precipitation (%) for the 2050s and 2080s

Figure 15 shows a detailed analysis of mean annual precipitation for the 2050s for each of the nine groups. The Northern regions receive less precipitation than the average across the whole study area. The region west of Metro Milwaukee also receives slightly less precipitation than the RP of the study area. For Metro Milwaukee the predicted results are different based on the emission scenarios. For the A1B the precipitation is lower than the average of the whole study area. For the A2 and B1 scenarios, the annual precipitation for Metro Milwaukee is predicted to be slightly higher than the RP of the whole study area. The southern regions receive more precipitation than the average over the whole study area. Overall, the predicted results for the 2050s show a larger discrepancy than was observed for the 1950 – 2006 period.
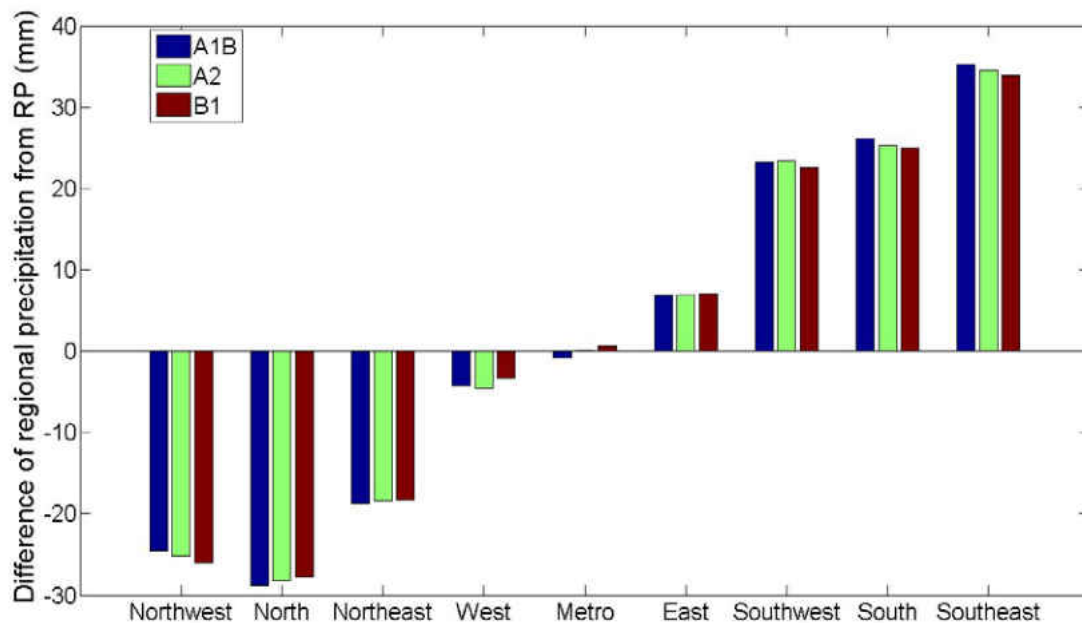
Fig. 15: Projected difference of regional precipitation from RP from 1950-2006 to the 2050s

Figure 16 shows a detailed analysis of mean annual precipitation for the 2080s for each of the nine groups. The northern areas are still projected to receive much less precipitation than the average across the study area, and for the southern regions much more than the average. For the A1B emission scenario the precipitation for each of the

groups stays very similar except for Metro Milwaukee. Here, the annual precipitation is predicted to be much lower than the average, and the difference is projected to be greater. For the A2 scenario, Metro Milwaukee seems to receive slightly more than the average, whereas for the B1 scenario the annual precipitation is just below the average of the study area. For the A2 and B1 emission scenarios the annual precipitation difference between each group and the average across the whole study area seems to deviate even more than for the 2050s.
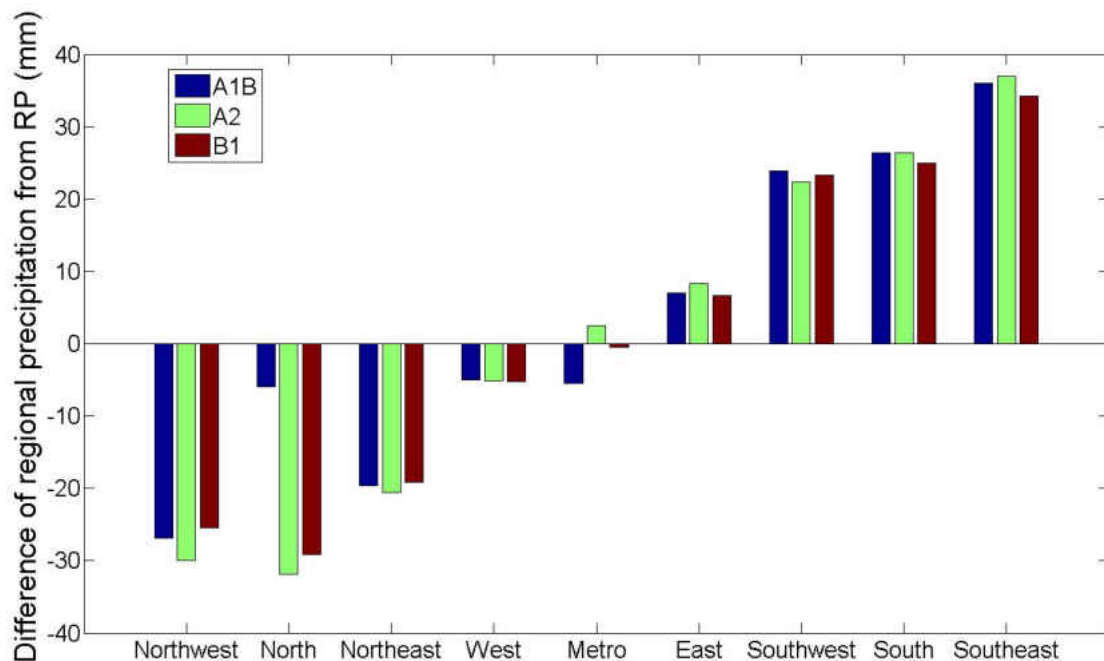
Fig. 16: Projected difference of regional precipitation from RP from 1950-2006 to the 2080s

7.3   Monthly Precipitation

The monthly precipitation for the current time period (1950-2006) and the 2050s for all three emission scenarios are presented in Figure 17. The annual variation of monthly precipitation for the 2050s is very similar to that of the current time period. For the cooler half of the year less precipitation is predicted, and higher monthly precipitation

totals are projected for the warmer half of the year. The lowest monthly totals are predicted to occur in February for all three scenarios. The lowest precipitation is projected in February with 28 mm for the A1B and B1 scenarios and 29 mm for the A2 scenario. The highest precipitation in September with 128 mm for the A1B scenario, and in April with 120 mm and 116 mm for the A2 and B1 scenarios respectively. For the A1B scenario the distribution of monthly precipitation for the months from October to March is predicted to be very similar to the current time period and does not change much. The warmer half of the year is projected to experience increases in mean monthly precipitation in some months and decreases in others. High monthly precipitation totals are predicted in April, which drop to slightly lower precipitation totals in May and June, and are then projected to steadily increase until the highest monthly precipitation is reached in September. The annual distribution of monthly precipitation totals is similar for the A2 and B1 scenarios. The April precipitation is projected to have the highest monthly totals in both scenario projections. The A2 scenario is projected to receive higher September precipitation totals than in August. The B1 scenario is projected to have higher precipitation amounts in August than in September.
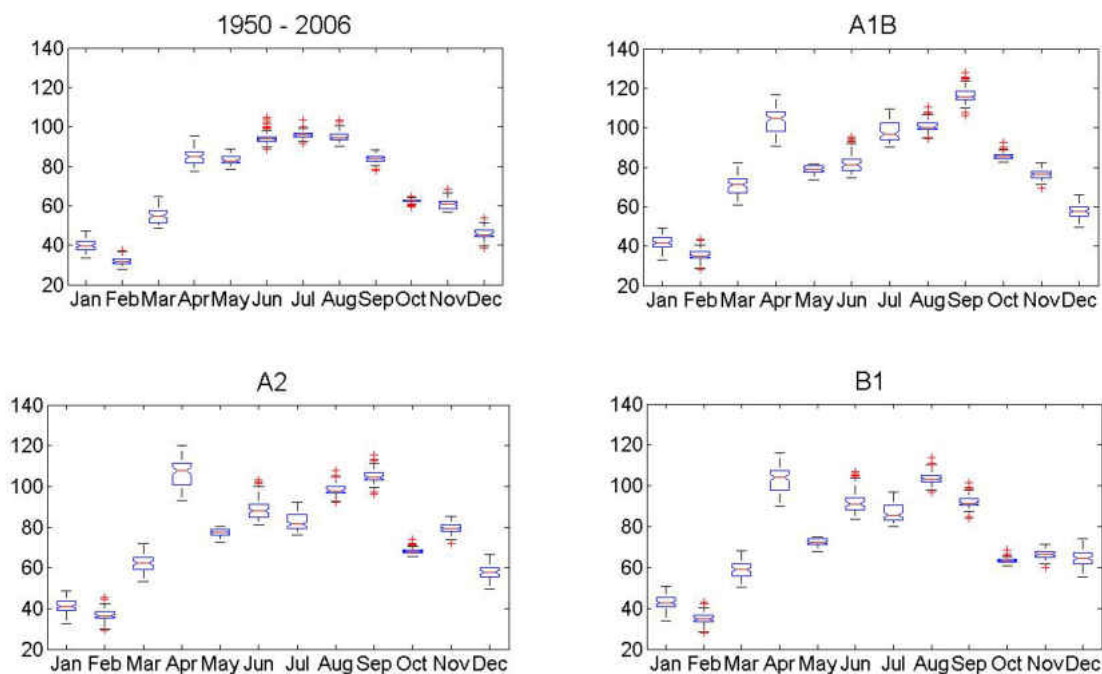
Fig. 17: Mean monthly precipitation (mm) for 1950-2006 and the 2050s for the A1B, A2 and B1 emission scenarios

Figure 18 presents the monthly precipitation for the current time and the 2080s. The annual variation of monthly precipitation totals throughout the year is very similar to the 2050s for all three emission scenarios. The projected monthly precipitation amount is less during winter and more during summer. The summer months for all three emission scenarios are projected to further decrease from the 2050s to the 2080s. A large increase can be found for April and September and a large decrease in October for all three emission scenarios. The August precipitation varies largely between the three emission scenarios.
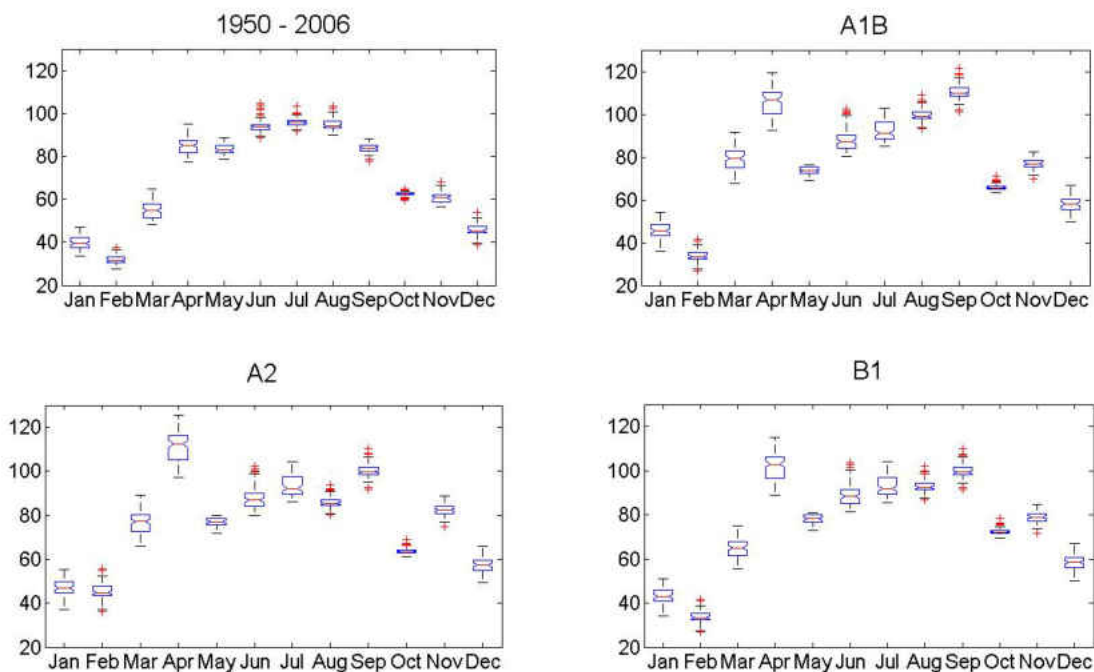
Fig. 18: Mean monthly precipitation (mm) for 1950-2006 and the 2080s for the A1B, A2 and B1 emission scenarios

The change of representative monthly precipitation from the current time period to the 2050s for all three emission scenarios is shown in figure 19. The precipitation for August to April is projected to increase; a decrease is predicted for May to July. The projected monthly precipitation changes are very inhomogeneous. Overall, the lowest change in precipitation is projected for the B1 emission scenario, and the largest change for the A1B emission scenario. The mean monthly precipitation is projected to increase for winter (December, January, February), spring (March, April, May) and fall (September, October, November). In summer (June, July, August) the monthly precipitation is projected to decrease with -3% for the A1B emission scenario, -6% for the A2 scenario, and -2% for the B1 scenario. In winter, the precipitation is projected to increase by 15% for the A1B and A2 scenarios, and 20% for the B1 scenario. In spring, the highest increase is projected for the A1B scenario with 15%, followed by 11% for the

A2 scenario, and the lowest increase for the B1 scenario with 5%. The precipitation increase in fall ranges from 34% (A1B scenario) to 7% (B1 scenario).
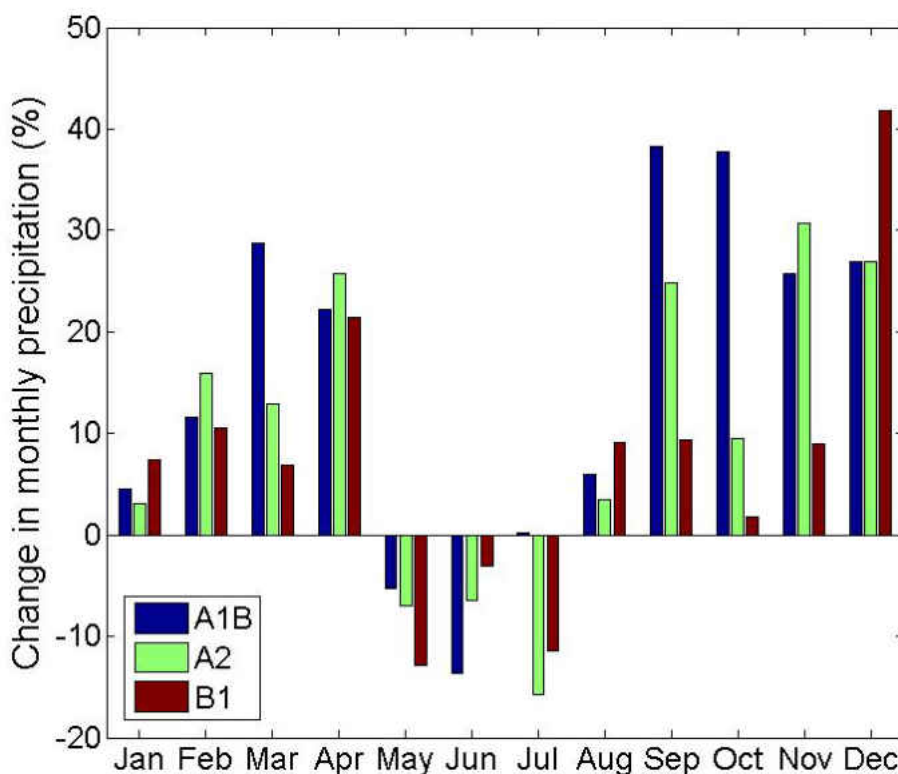
Fig. 19: Changes in representative mean monthly precipitation for the 2050s for the A1B, A2, and B1 scenario

The projected representative monthly precipitation for the 2080s for all three emission scenarios is shown in Figure 20. The precipitation in winter, fall, and spring is projected to increase, but the summer precipitation is projected to decrease. The projected changes are of the same direction, either increasing or decreasing, for all months expect August. The precipitation changes for August are projected to increase by 5% for the A1B scenario, and to decrease by 10% and 3% for the A2 and B1 scenarios respectively. The monthly changes in precipitation amount are very different based on the underlying emission scenario. The winter precipitation is projected to increase by 16% for the A1B, 29% for the A2, and 14% for the B1 emission scenario. In spring, the precipitation is projected to increase by 11% to 21%, and the increases in fall precipitation range from

19% to 21%. The summer precipitation is projected to decrease by -7% for the A2 scenario, by -4% for the B1 scenario and by -1% for the A1B scenario.
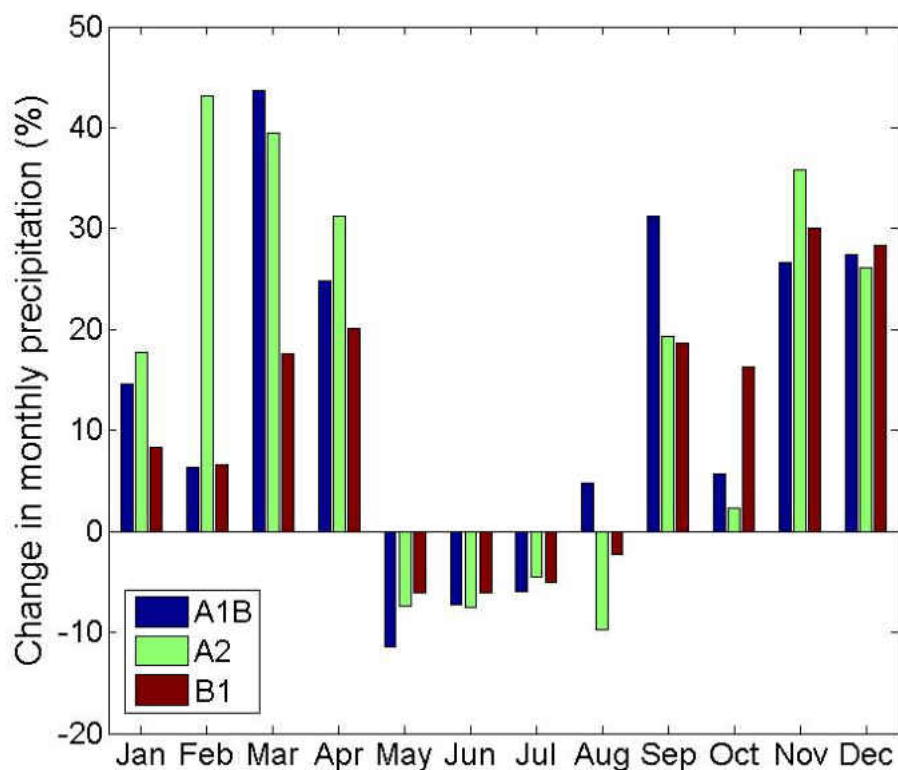
Fig 20: Changes in representative mean monthly precipitation for the 2080s for the A1B, A2, and B1 scenario

The spatial distribution of mean monthly precipitation for the 2050s based on the A1B, A2, and B1 emission scenarios are shown in Figure 21. The projected spatial distributions for all three emission scenarios are very similar. From November to April the highest precipitation is projected in the southeast corner, reaching into the southeastern regions of the study area. The highest precipitation is projected in the southern parts of the study area in May, and in the southwestern corner in June, July, and August. In September and October the highest precipitation is projected to occur in the northwestern corner. A center of low precipitation over Metro Milwaukee is projected in June, July, August, September, and October. The projected spatial distribution of

averaged monthly precipitation is very similar to the spatial distribution of mean monthly

precipitation for 1950 to 2006.

Fig. 21a: Spatial variation of projected mean monthly precipitation (mm) for the A1B emission scenario for the 2050s from January to June

July
- 90.3 - 93.5
- 93.6 - 96.8
- 96.9 - 100
- 100.1 - 103.2
- 103.3 - 106.4
- 106.5 - 109.6

August
- 94.3 - 97
- 97.1 - 99.7
- 99.8 - 102.3
- 102.4 - 105
- 105.1 - 107.7
- 107.8 - 110.3

September
- 106.4 - 110
- 110.1 - 113.7
- 113.8 - 117.3
- 117.4 - 120.9
- 121 - 124.5
- 124.6 - 128.2

October
- 82.4 - 84.1
- 84.2 - 85.8
- 85.9 - 87.5
- 87.6 - 89.2
- 89.3 - 90.9
- 91 - 92.6

November
- 69.2 - 71.4
- 71.5 - 73.5
- 73.6 - 75.6
- 75.7 - 77.7
- 77.8 - 79.8
- 79.9 - 82

December
- 49.6 - 52.4
- 52.5 - 55.2
- 55.3 - 58
- 58.1 - 60.7
- 60.8 - 63.5
- 63.6 - 66.3

Fig. 21b: Spatial variation of projected mean monthly precipitation (mm) for the A1B emission scenario for the 2050s for July to December

Fig. 21c: Spatial variation of projected mean monthly precipitation (mm) for the A2 emission scenario for the 2050s for January to June

July
- 75.9 - 78.6
- 78.7 - 81.3
- 81.4 - 84
- 84.1 - 86.7
- 86.8 - 89.4
- 89.5 - 92.1

August
- 92 - 94.6
- 94.7 - 97.2
- 97.3 - 99.8
- 99.9 - 102.4
- 102.5 - 105.1
- 105.2 - 107.7

September
- 96 - 99.3
- 99.4 - 102.6
- 102.7 - 105.9
- 106 - 109.1
- 109.2 - 112.4
- 112.5 - 115.7

October
- 65.5 - 66.9
- 67 - 68.2
- 68.3 - 69.6
- 69.7 - 70.9
- 71 - 72.3
- 72.4 - 73.6

November
- 72 - 74.2
- 74.3 - 76.4
- 76.5 - 78.6
- 78.7 - 80.9
- 81 - 83.1
- 83.2 - 85.3

December
- 49.6 - 52.4
- 52.5 - 55.2
- 55.3 - 57.9
- 58 - 60.7
- 60.8 - 63.5
- 63.6 - 66.3

Fig. 21d: Spatial variation of projected mean monthly precipitation (mm) for the A2 emission scenario for the 2050s for July to December

January
- 33.7 - 36.6
- 36.7 - 39.4
- 39.5 - 42.2
- 42.3 - 45
- 45.1 - 47.8
- 47.9 - 50.6

February
- 28 - 30.5
- 30.6 - 33
- 33.1 - 35.5
- 35.6 - 38.1
- 38.2 - 40.6
- 40.7 - 43.1

March
- 50.4 - 53.3
- 53.4 - 56.3
- 56.4 - 59.3
- 59.4 - 62.3
- 62.4 - 65.2
- 65.3 - 68.2

April
- 90 - 94.4
- 94.5 - 98.7
- 98.8 - 103.1
- 103.2 - 107.4
- 107.5 - 111.8
- 111.9 - 116.1

May
- 67.7 - 68.9
- 69 - 70.2
- 70.3 - 71.4
- 71.5 - 72.7
- 72.8 - 73.9
- 74 - 75.1

June
- 83.8 - 87.7
- 87.8 - 91.6
- 91.7 - 95.5
- 95.6 - 99.3
- 99.4 - 103.2
- 103.3 - 107.1

Fig. 21e: Spatial variation of projected mean monthly precipitation (mm) for the B1 emission scenario for the 2050s for January to June

July
- 79.88 - 82.72
- 82.721 - 85.57
- 85.571 - 88.41
- 88.411 - 91.26
- 91.261 - 94.1
- 94.101 - 96.95

August
- 97.08 - 99.83
- 99.831 - 102.57
- 102.571 - 105.32
- 105.321 - 108.06
- 108.061 - 110.81
- 110.811 - 113.56

September
- 84.15 - 87.01
- 87.011 - 89.88
- 89.881 - 92.74
- 92.741 - 95.61
- 95.611 - 98.47
- 98.471 - 101.34

October
- 60.90 - 62.16
- 62.161 - 63.42
- 63.421 - 64.68
- 64.681 - 65.94
- 65.941 - 67.2
- 67.201 - 68.46

November
- 60.05 - 61.89
- 61.891 - 63.74
- 63.741 - 65.58
- 65.581 - 67.43
- 67.431 - 69.27
- 69.271 - 71.13

December
- 55.45 - 58.55
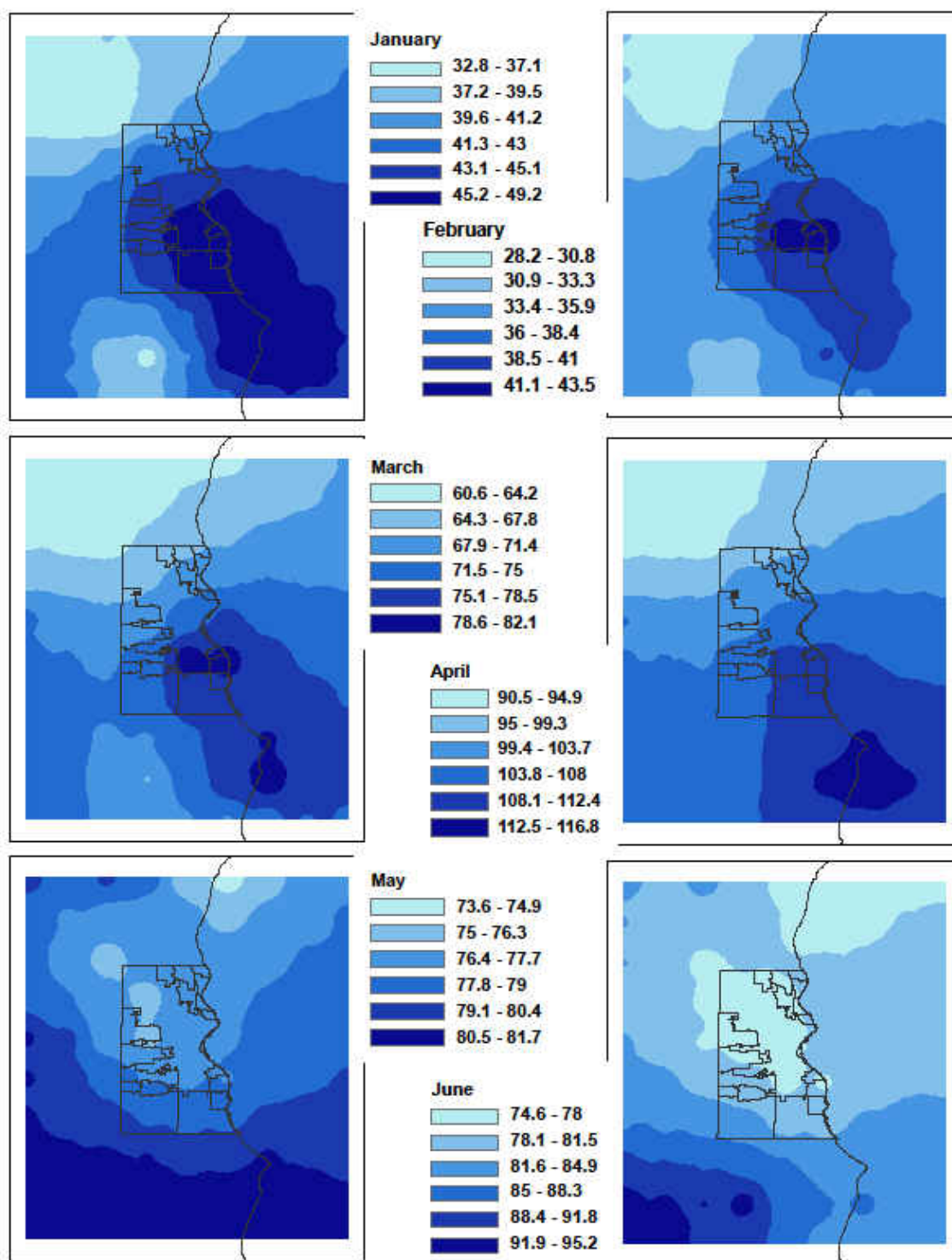- 58.551 - 61.65
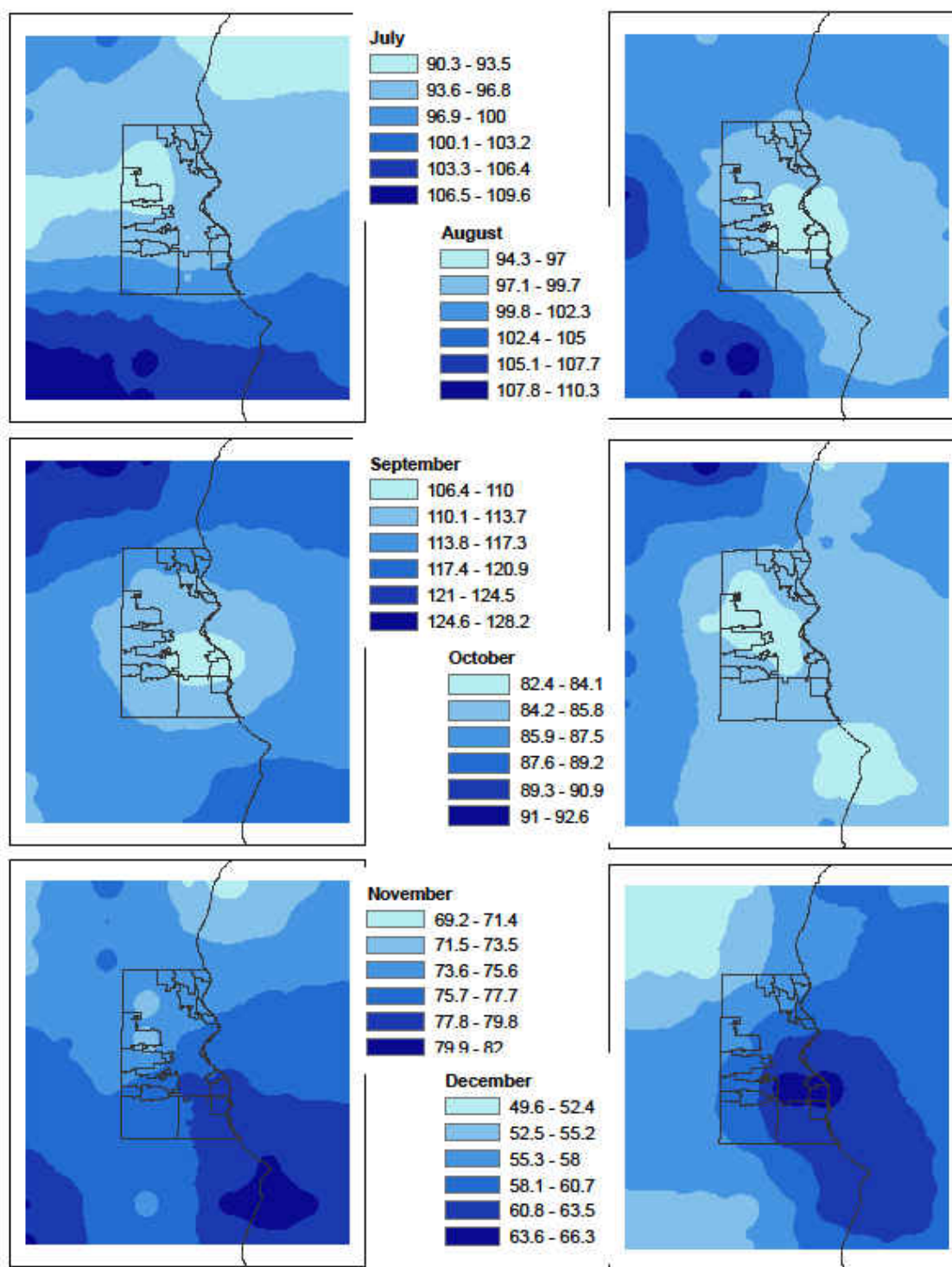- 61.651 - 64.75
- 64.751 - 67.85
- 67.851 - 70.95
- 70.951 - 74.06

Fig. 21f: Spatial variation of projected mean monthly precipitation (mm) for the B1 emission scenario for the 2050s for July to December

The spatial distribution of mean monthly precipitation for the 2080s based on the A1B, A2, and B1 emission scenarios are shown in Figure 22. The projected spatial distributions for all three emission scenarios are very similar. From November to April the highest precipitation is projected in the southeast corner reaching into the southeastern region of the study area. The highest precipitation is projected in the southern parts of the study area in May and in the southwestern corner in June, July, and August. In September and October the highest precipitation is projected to fall in the northwestern corner. A center of low precipitation over Metro Milwaukee is projected in June, July, August, September, and October. The projected spatial distribution of averaged monthly precipitation is very similar to the spatial distribution of mean monthly precipitation for 1950 to 2006.

Fig. 22a: Spatial variation of projected mean monthly precipitation (mm) for the A1B emission scenario for the 2080s for January to June

Fig. 22b: Spatial variation of projected mean monthly precipitation (mm) for the A1B emission scenario for the 2080s for July to December
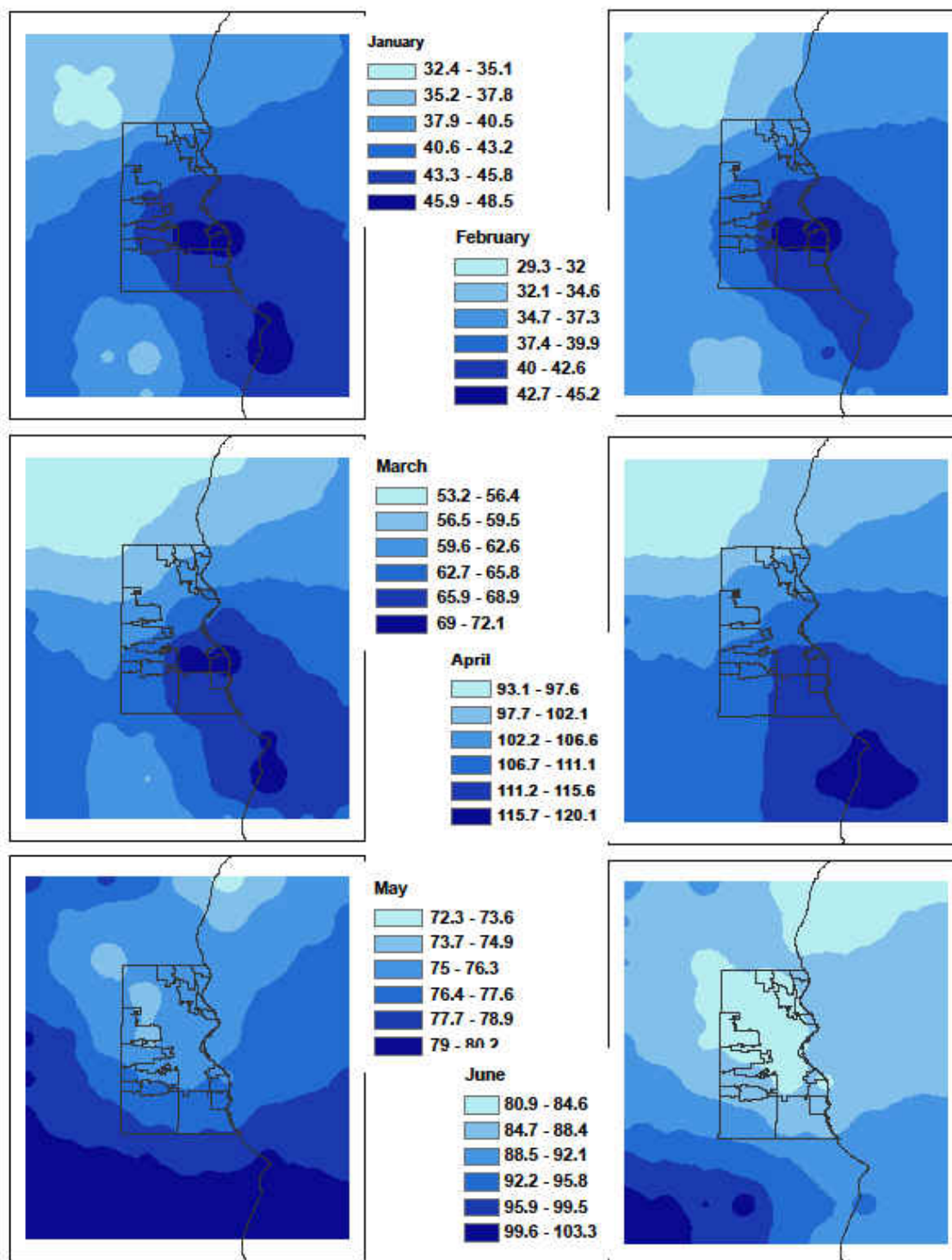
Fig. 22c: Spatial variation of projected mean monthly precipitation (mm) for the A2 emission scenario for the 2080s for January to June
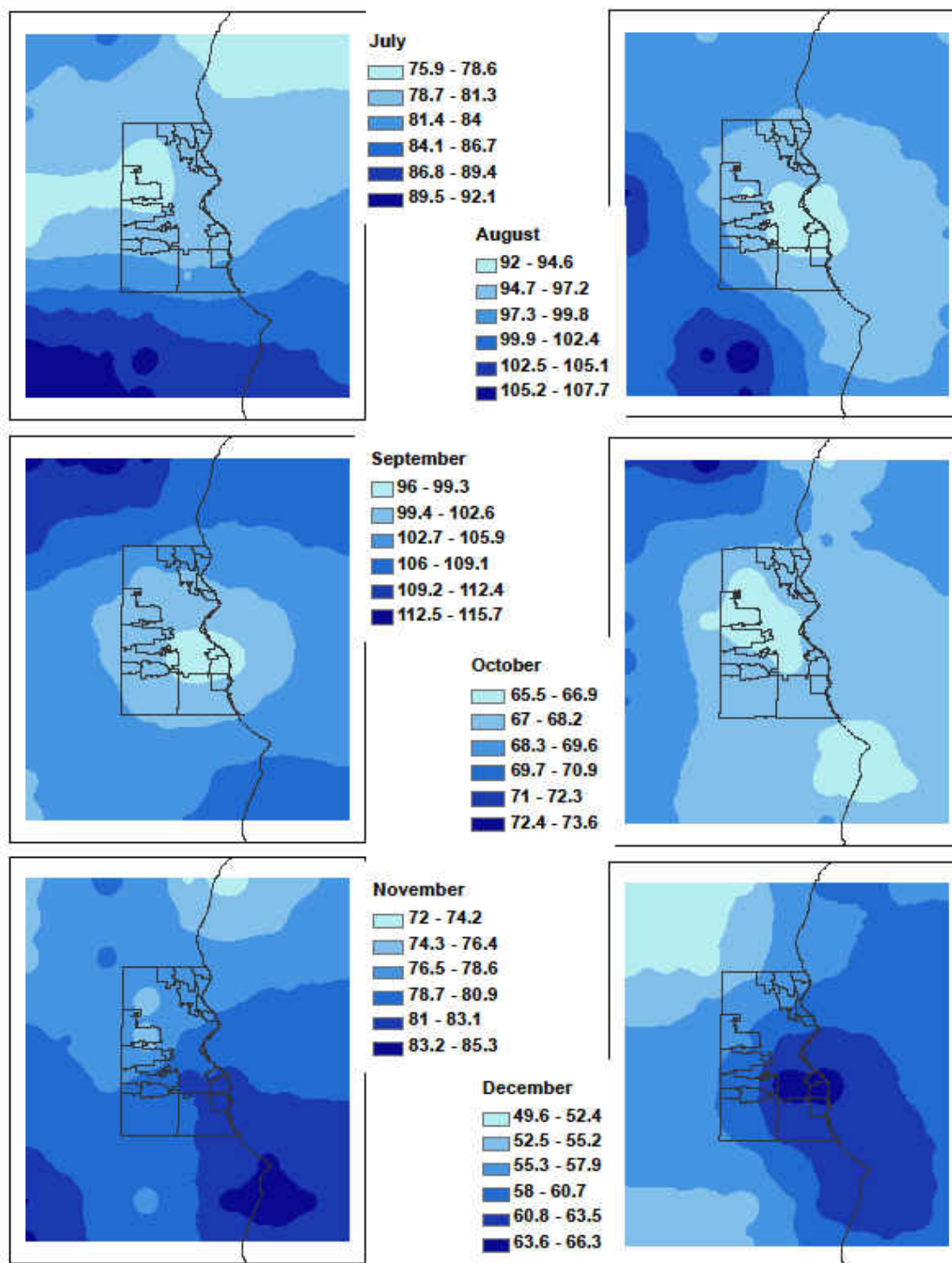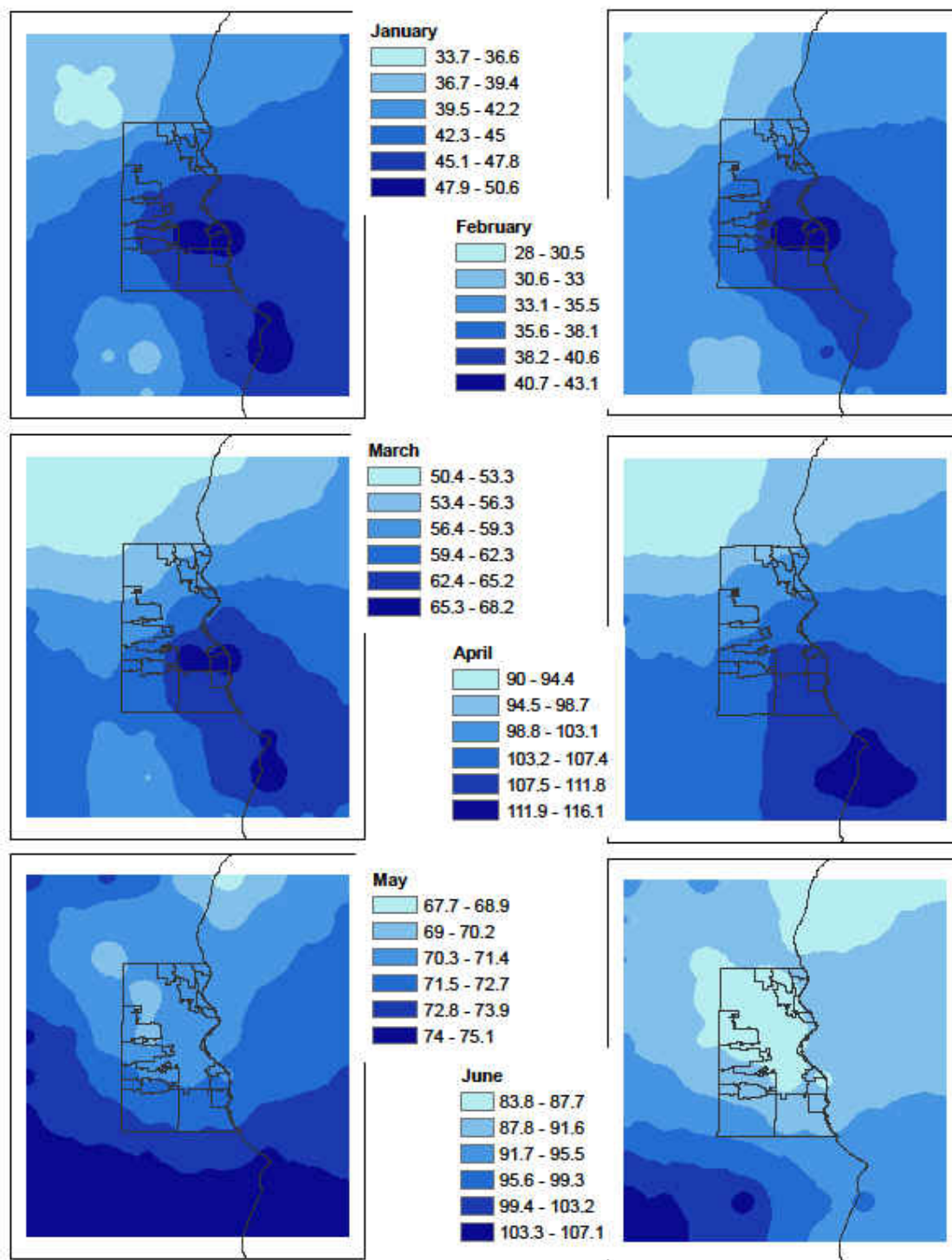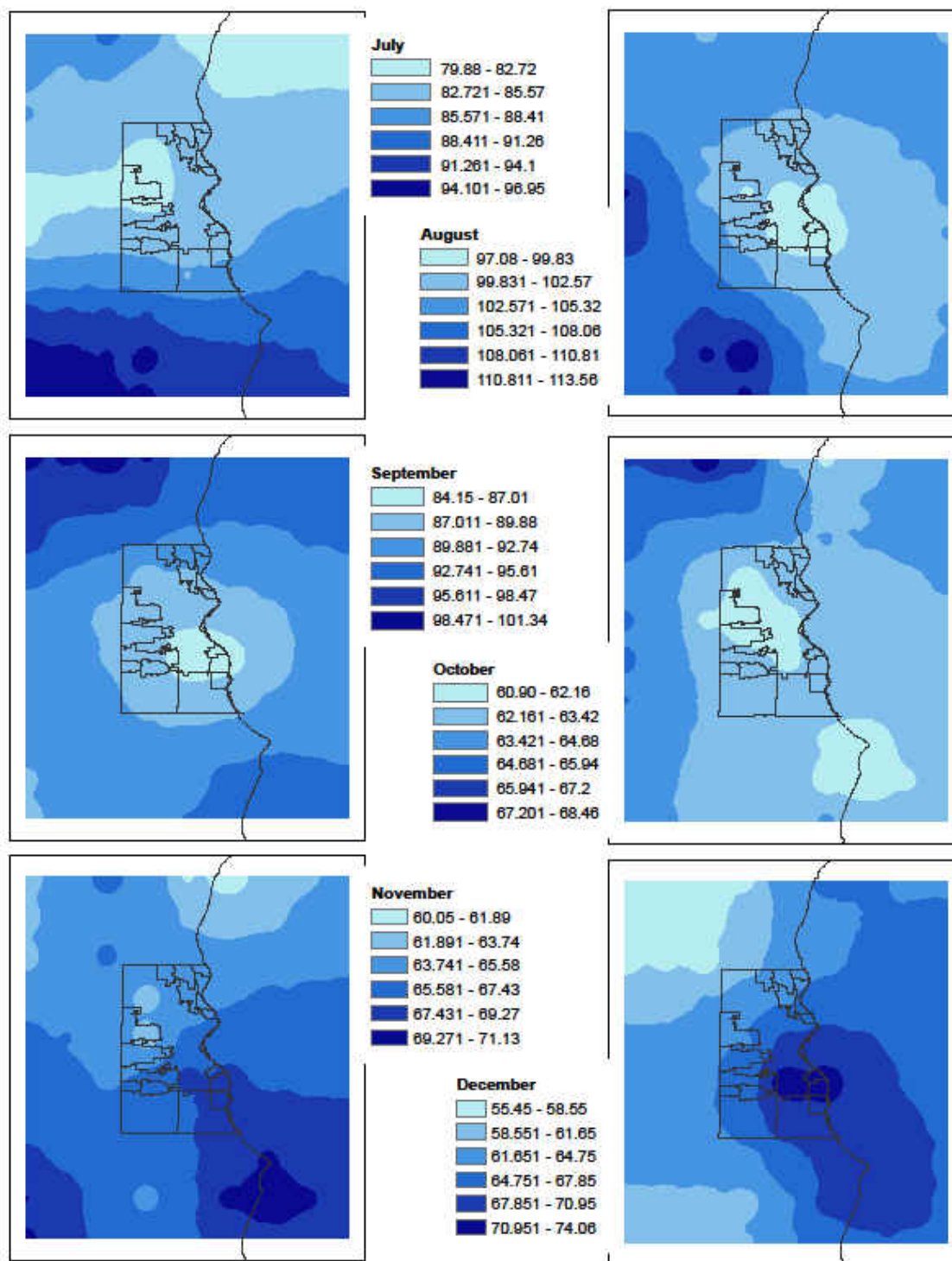
Fig. 22d: Spatial variation of projected mean monthly precipitation (mm) for the A2 emission scenario for the 2080s for July to December
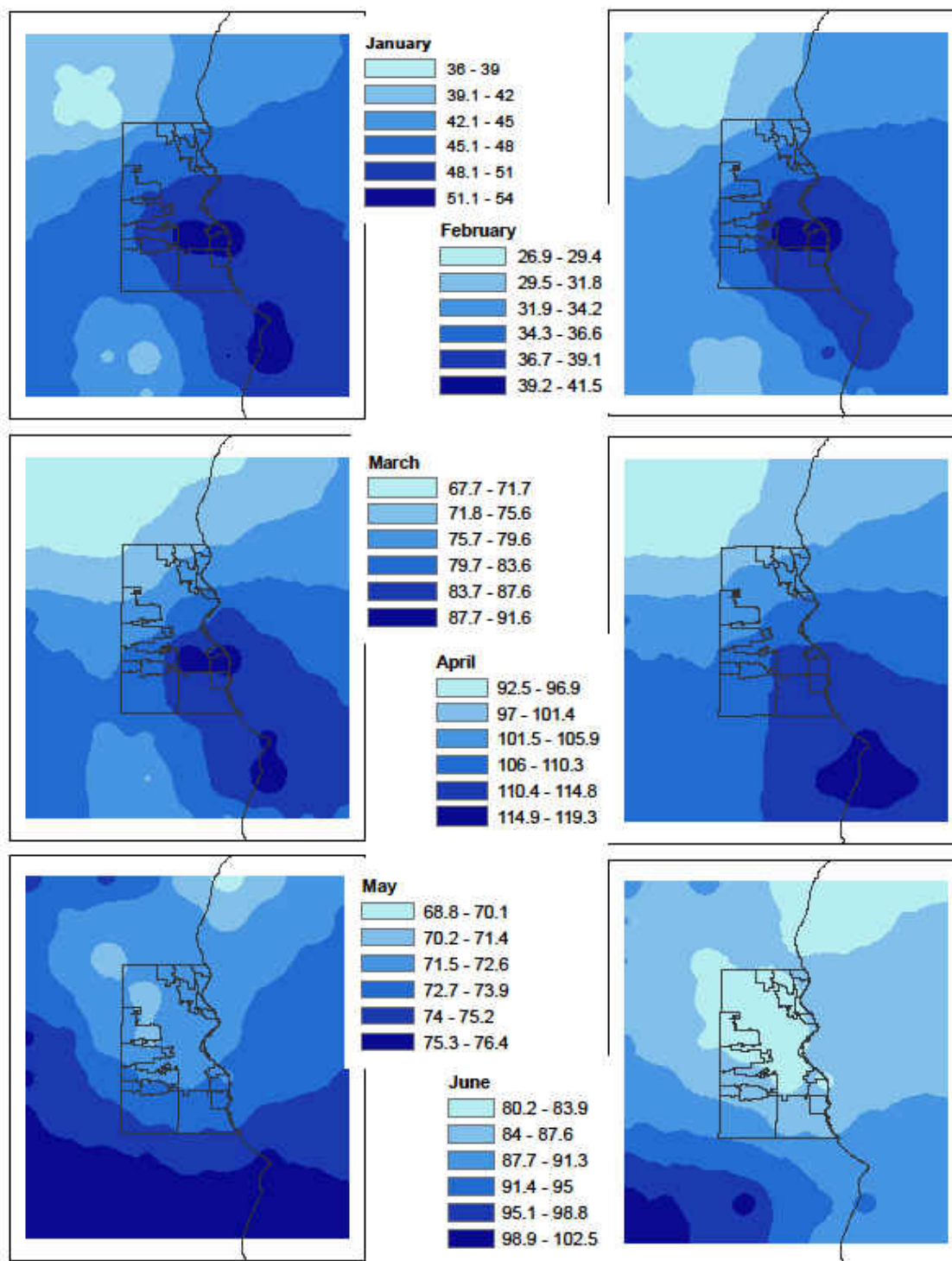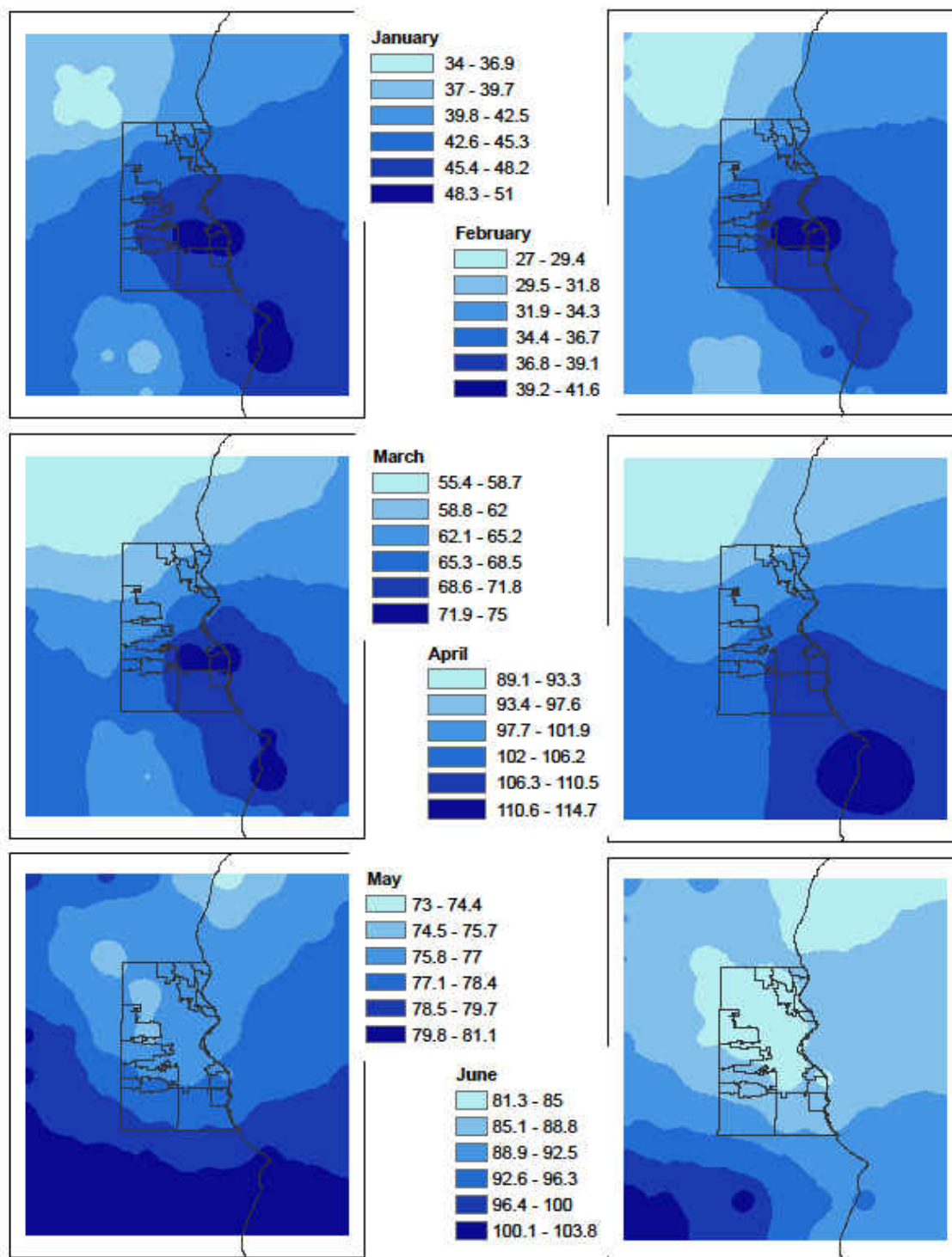
Fig. 22e: Spatial variation of projected mean monthly precipitation (mm) for the B1 emission scenario for the 2080s for January to June
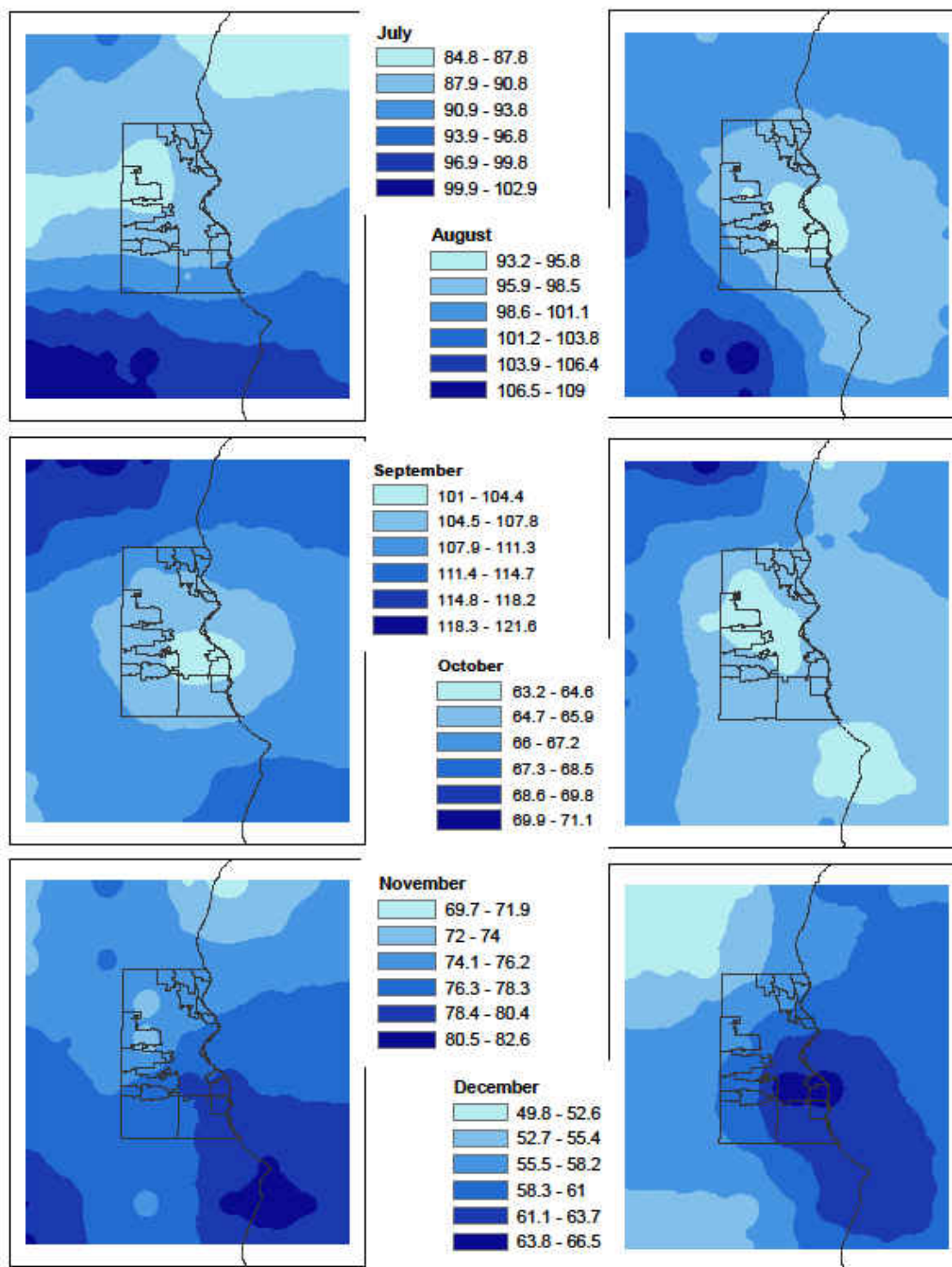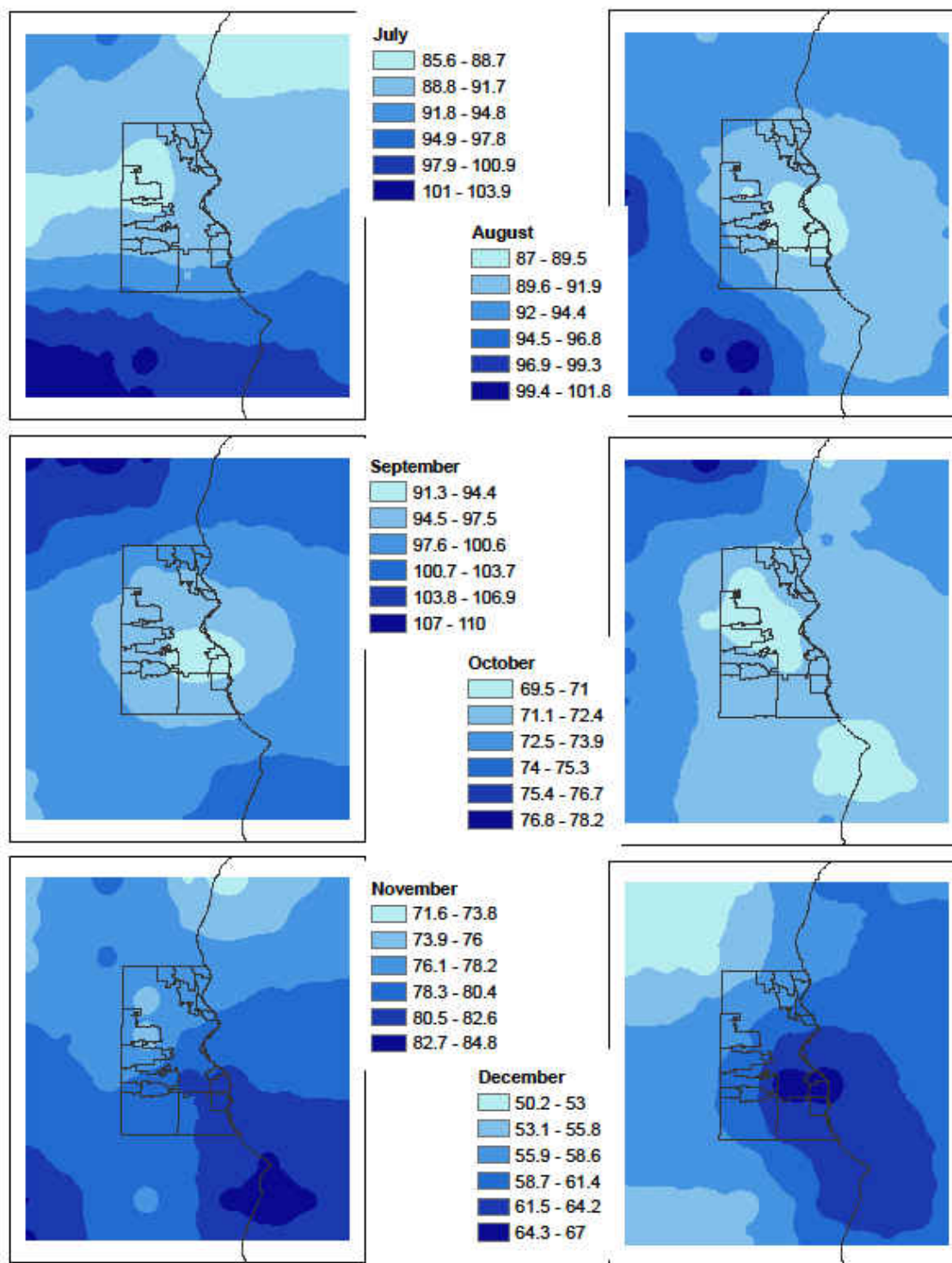
Fig. 22f: Spatial variation of projected mean monthly precipitation (mm) for the B1 emission scenario for the 2080s for July to December
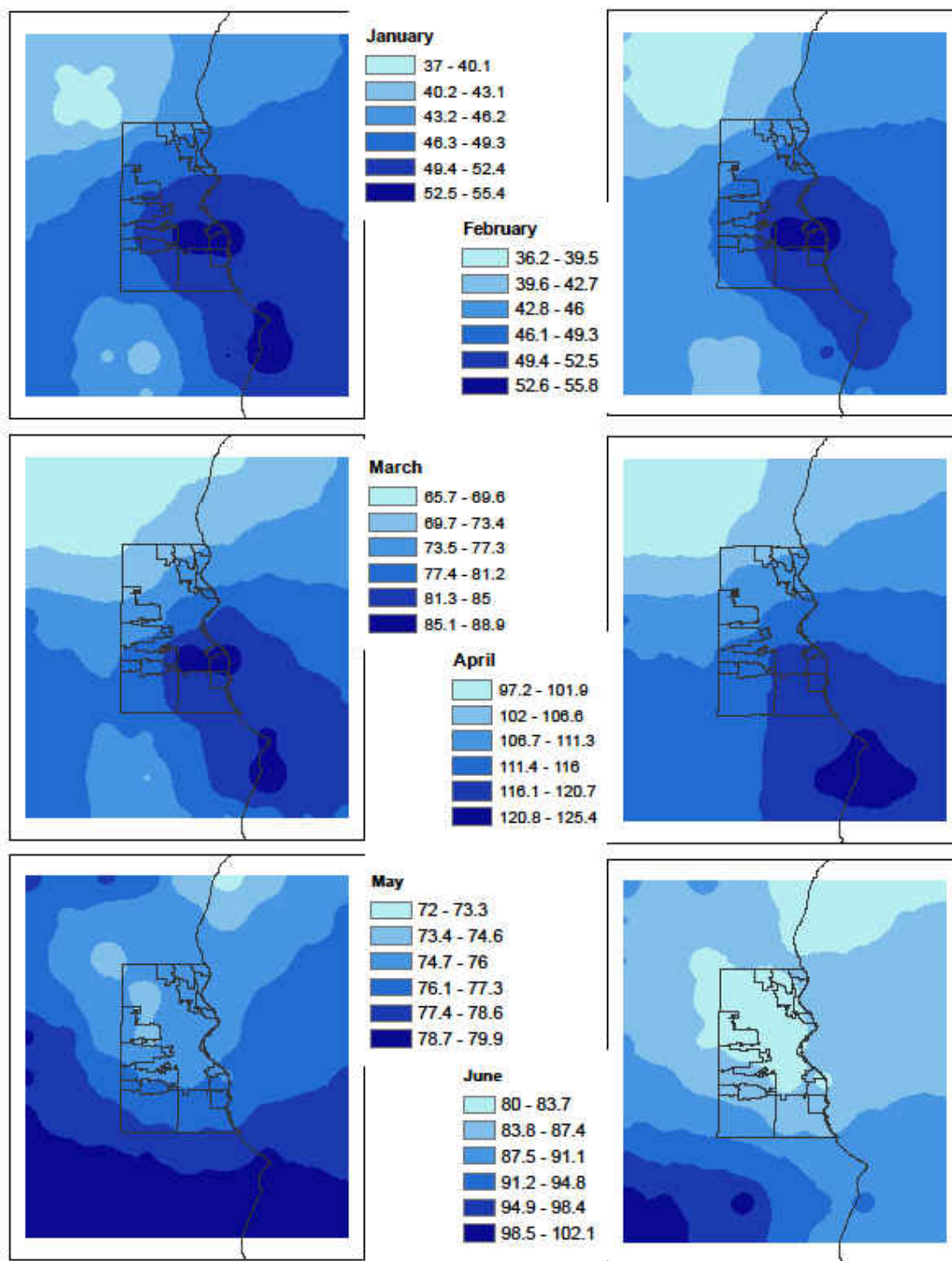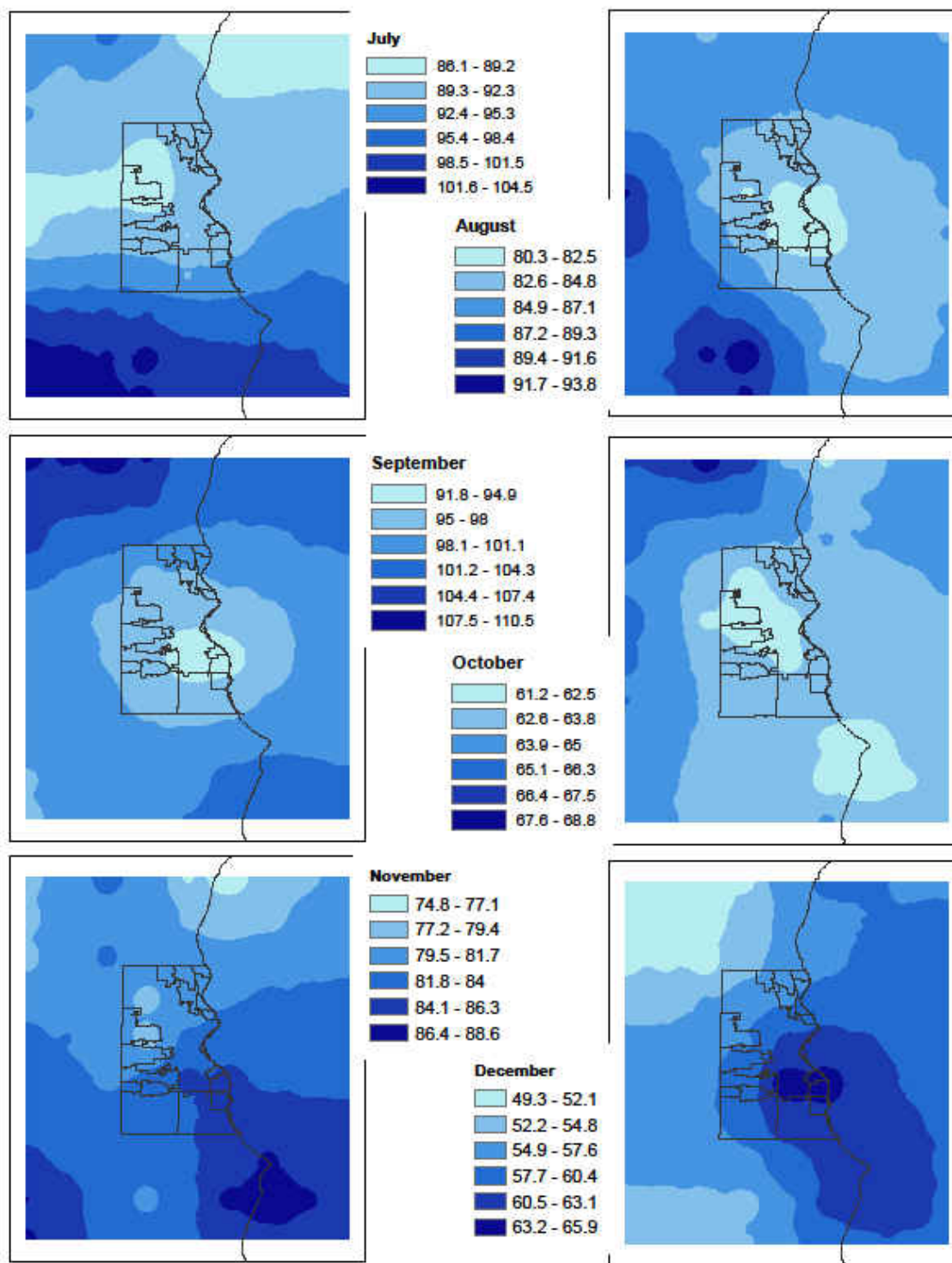
7.4   Extreme Precipitation

Changes in the representative 95th percentile precipitation are presented in Figure 23. The 95th percentile of annual precipitation changes from the current time (1950 to 2006) to the 2050s by 30% for the A1B and B1 emission scenarios and by 29% for the A2 scenario. The changes from the current time period to the 2080s are projected to be similar with 29% for the A1B scenario and 30% for the A2 and the B1 emission scenarios. The two-sample t-test, as available in MATLAB as the 'ttest2' function, was used to analyze the significance of these changes in 95th percentile precipitation. The changes for all three emission scenarios for the 2050s and 2080s were of significance at the 95 percent confidence interval.

The changes projected for the 95th percentile precipitation for the 2050s and 2080s are higher than the changes for the annual mean precipitation. The annual mean precipitation changes for the 2050s range from 6% to 14% and from 9% to 12% for the 2080s (for more details see chapter 7.2). The percentage changes for the 95th percentile precipitation are much higher with 29% to 30% for the 2050s and the 2080s. In both cases the 2080s are projected to increase more than the 2050s with the exception of the A1B scenario. In this case, the 2050s show a slightly larger increase than the 2080s. The percentage differences between the emission scenarios are stronger for the 2050s than the 2080s for the projected annual precipitation and almost the same for the 95th percentile precipitation.
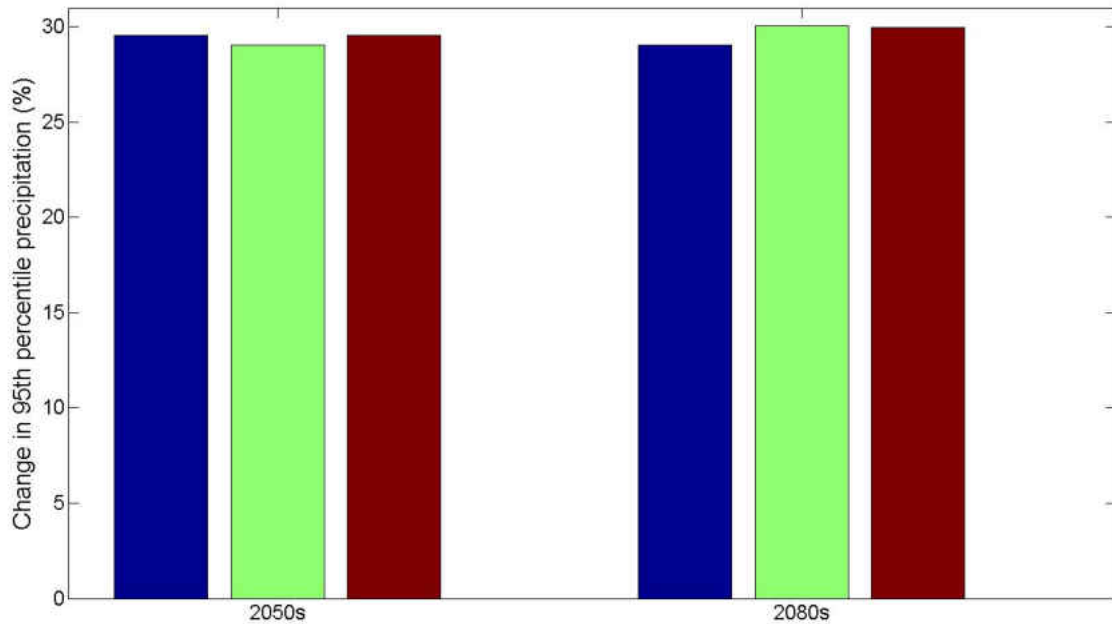
Fig 23: Changes in 95th percentile precipitation from 1950-2006 to the 2050s and 2080s

The spatial variation of 95th percentile precipitation for the A1B emission scenario ranges from 19% to 40% for the 2050s and from 16% to 37% for the 2080s (Fig. 24). For the A2 emission scenario the 95th percentile precipitation ranges from 16% to 40% for the 2050s and from 21% to 46% for the 2080s. The B1 emission scenario is projected to range from 20% to 40% for the 2050s and from 19% to 43% for the 2080s. The spatial variation varies between the three emission scenarios and does not show a distinctive pattern. In all three emission scenarios, the highest percentage changes in 95th percentile precipitation are projected in Metro Milwaukee. The extent of the area showing the largest increases in extreme precipitation vary among the emission scenarios as well as the two time frames.

A1B 2050s
	19.4 - 22.8
	22.9 - 26.2
	26.3 - 29.7
	29.8 - 33.1
	33.2 - 36.5
	36.6 - 39.9

A1B 2080s
	16.1 - 19.7
	19.8 - 23.2
	23.3 - 26.8
	26.9 - 30.3
	30.4 - 33.8
	33.9 - 37.4

A2 2050s
	15.8 - 19.8
	19.9 - 23.8
	23.9 - 27.7
	27.8 - 31.7
	31.8 - 35.7
	35.8 - 39.6

A2 2080s
	21.3 - 25.5
	25.6 - 29.6
	29.7 - 33.7
	33.8 - 37.8
	37.9 - 41.9
	42 - 46

B1 2050s
	19.9 - 23.2
	23.3 - 26.5
	26.6 - 29.7
	29.8 - 33
	33.1 - 36.3
	36.4 - 39.6

B1 2080s
	18.7 - 22.7
	22.8 - 26.6
	26.7 - 30.6
	30.7 - 34.6
	34.7 - 38.5
	38.6 - 42.5

Fig. 24: Changes of 95th percentile of annual precipitation (%) for the A1b, A2, and B1 emission scenario from 1950-2006 to the 2050s and to the 2080s

Chapter 8: Discussion

8.1   Decadal Changes in Precipitation

The averaged annual precipitation for Metro Milwaukee and the surrounding areas of 831 mm is slightly higher than the averaged annual precipitation of the larger southeastern corner of Wisconsin as shown by Serbin and Kucharik (2009). This f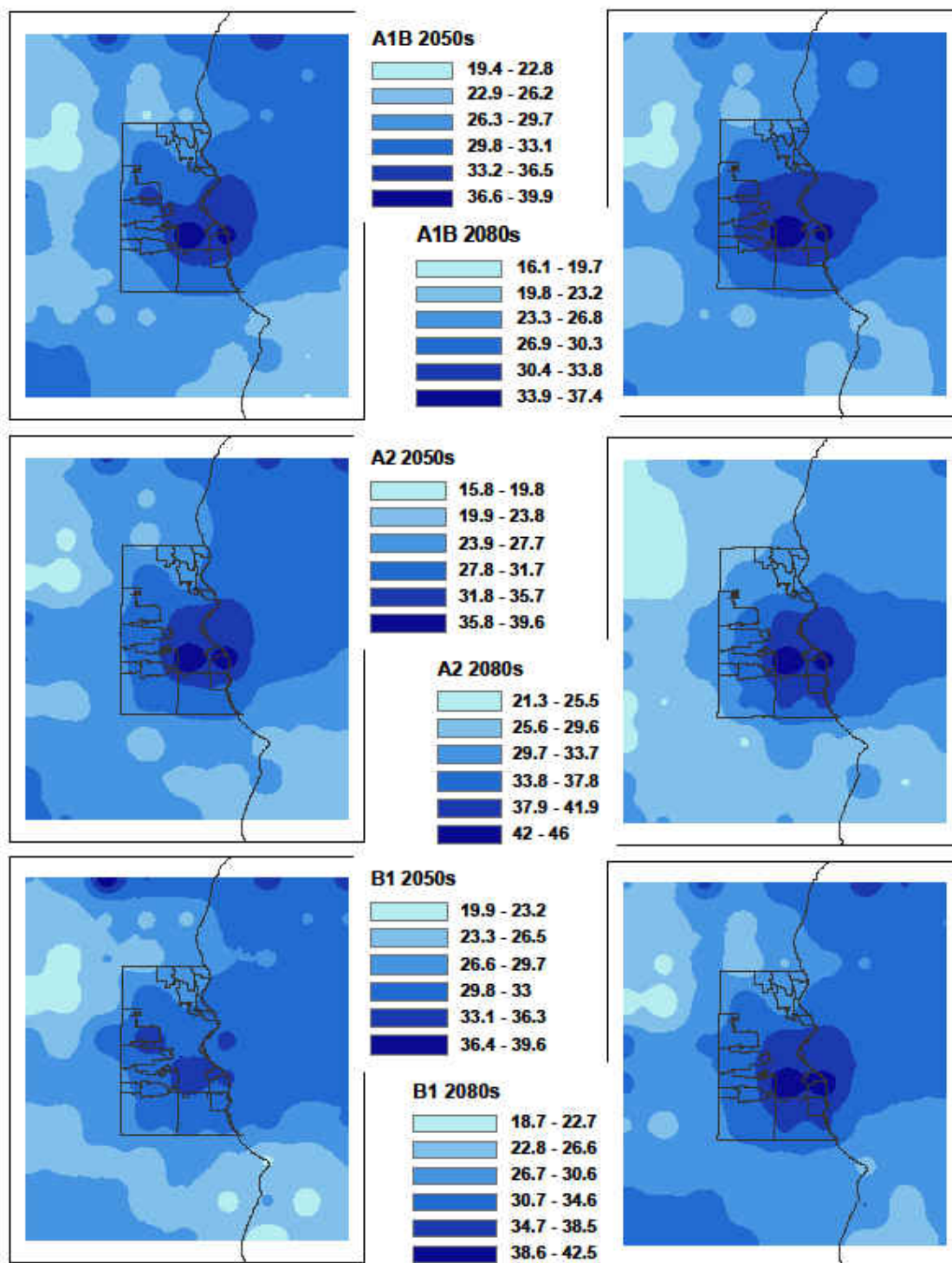its with the findings by Serbin and Kucharik (2010a) which found that the annual precipitation totals for the southern regions are higher than those for the northern areas with a latitudinal decrease. As the larger southeastern corner of Wisconsin reaches further north than the study area, it is to be expected that the average annual precipitation in this study is slightly higher than that of the larger southeastern corner of Wisconsin. A spatial analysis of winter and summer precipitation shows that the Milwaukee county area receives higher precipitation amounts than the average of the southeastern corner of the state.

The results of the annual precipitation trend should be interpreted with some caution due to the restricted time period of 56 years (1950-2006). Some variation in magnitude of trends would result if a different time period were analyzed. Kucharik et al. (Kucharik et al. 2010a) found a significant increasing trend for the southwestern corner of Wisconsin at a 90 percent confidence interval. The results for this study only show a significant trend for the northern and western parts, this might be because of a smaller confidence interval (95 percent confidence) or due to the smaller study area. The spatial variation in increasing precipitation trends found in this study are very similar to those presented in the first report of the Wisconsin Initiative on Climate Change Impacts (Wisconsin Initiative on Climate Change Impact 2011).

8.2   Effects of Metro Milwaukee on Precipitation

Many studies have found an increase in precipitation of varying degree on the downwind side of urban areas. Huff and Changnon (1973) found that for six large U.S. cities urban induced precipitation increases of 10-30%, in and downwind of the city, occurred for the time period 1955-1970. Dixon and Mote (2003) found similar results for Atlanta, Georgia. The UHI has been shown to enhance and possibly initiate thunderstorms and thunderstorm related precipitation. Most of these events occurred at night and near high-density urban areas. This study is based on daily precipitation data and therefore does not focus on the time of the day at which the precipitation events occur. Only changes in the precipitation amount are analyzed.

To analyze if increased precipitation downwind of the city also occurs for Milwaukee annual and monthly averages of the predominant wind directions were obtained from the Wisconsin State Climatology office (http://www.aos.wisc.edu/~sco/climhistory/stations/mke/milwind.html). Table 5 shows the average monthly and annual wind direction for wind data at Milwaukee, Wisconsin for the time period 1948 to 1990.

Based on the spatial analysis of averaged annual precipitation amounts, the highest precipitation is predicted in the southeastern regions of the study area and the lowest in the northwestern and northern regions. The highest average annual precipitation is located downwind of Metro Milwaukee. The averaged annual wind is a west-northwest wind (Table 5). The high precipitation located to the southeast of the study area could be partially due to the urban effects enhancing the precipitation magnitude. Similar patterns can also be found for the monthly precipitation. In winter (December - February) high

precipitation amounts are shown in the southeastern portion of Metro Milwaukee and in the southeastern parts of the study area. The predominant wind direction in winter is west-northwest. In March and April the wettest areas are found in the southeastern corner of the study area. In May the highest precipitation is occurs in the southern regions. The predominant wind pattern for March is west-northwest which could explain the high center of precipitation southeast of Metro Milwaukee. In April and May the wind predominantly comes from the north-northeast. This might explain the shift from the concentrated high precipitation in the southeastern corner towards the more widespread precipitation in the southern regions. In June the highest precipitation can be found in the southwest and the predominant wind direction is north-northeast. This once again puts the highest precipitation amounts at the downwind side of Metro Milwaukee. In July to September the wind is predominantly coming from the southwest and south-southwest. During these months the highest precipitation can be found in the southwest and western regions. In November the predominant wind is again coming from the west-northwest and the southeastern regions experience the highest precipitation.

Table 5: Predominant wind direction based on annual and monthly averages for the time period 1948 - 1990

	Average wind direction
Annual	West-northwest
January	West-northwest
February	West-northwest
March	West-northwest
April	North-northeast
May	North-northeast
June	North-northeast
July	Southwest
August	Southwest
September	South-southwest
October	South-southwest
November	South-southwest
December	West-northwest

8.3   Projected Changes in Precipitation

The mean annual precipitation is projected to increase by 6% to 14% by the 2050s and by 9% to 12% by the 2080s. These results fall within the range of percentage changes found by the Wisconsin Initiative on Climate Change (2011), which suggest that the annually averaged precipitation will change by -5% and +15% by the mid 21st century, and by -5% and +25% by the end of the century, within the entire state of Wisconsin for the A1B emission scenario.

By the 2050s the monthly precipitation is projected to increase in winter, spring and fall for all emission scenarios, whereas the summer precipitation is projected to decrease. The seasonal precipitation is projected to increase in winter by 15% to 20%, in spring by 5% to 15%, and by 7% to 34% in fall. The summer precipitation is projected to decrease by -2% to -6%. The analysis of seasonal precipitation changes by the Wisconsin Initiative on Climate Change Impacts (2011) showed a suggested change of 0% to 40% in

winter, -5% to 25% in spring, 5% to 15% in fall, and -20 to 15% in summer for the mid 21st century. The averaged monthly precipitation changes for the A1B emission scenario in this study fall within the averages projected for the whole state of Wisconsin. The only exception is for the fall precipitation which is projected to be much higher than the average across Wisconsin.

This research focuses on the analysis of precipitation for the current time (1950-2006) and the mid and late 21st century for Metro Milwaukee and the surrounding area. A detailed analysis of changes in precipitation for Metro Milwaukee was not included by the Wisconsin Initiative on Climate Change Impacts (2011). The spatial variation across Metro Milwaukee and the surrounding areas are particularly interesting and very similar to the spatial pattern of the current time period. A detailed analysis suggests that the highest precipitation for the current time period occurs on the downwind site of the city. The centers of high precipitation on the downwind side for the current time period are projected to be larger and more intense in the future. Future research should be conducted to determine if the correlation between the highest precipitation amounts and the predominant wind directions will continue to occur in the future.

Chapter 9: Summary & Conclusions

The primary goals of this research were to spatially and temporally analyze precipitation from the high-resolution gridded historical climatic dataset for Wisconsin for the time period 1950-2006 in Metro Milwaukee, and to generate precipitation scenarios via statistical downscaling of global climate model outputs. The delta change method was chosen for statistical downscaling of the historical climatic dataset for Wisconsin for the two future time period 2041-2070 and 2071-2100. The annual, monthly and extreme precipitation for the current time period and the future were analyzed. To identify the trend of annual precipitation and the 95th percentile precipitation the Mann-Kendall test of trend and the Sen's slope test were applied. Spatial variations of precipitation characteristics were analyzed by spatially interpolating the data from each grid point with the inverse distance weighting interpolation algorithm.

The major findings are summarized as follows:

- The spatial variation of annual precipitation from 1950-2006 differs largely across the study region ranging from 798 mm to 889 mm. The highest precipitation is in the southeastern corner and the lowest precipitation in the northwestern region. A very similar spatial pattern of annual precipitation is projected in the future for all three emission scenarios, but with higher annual precipitation totals. The annual precipitation is projected to increase by 6% to 14% by the 2050s and by 8% to 12% by the 2080s.

- The regional differences in annual precipitation for 1950-2006 show that the northern regions receive less precipitation than the average across the whole study area, while

the southern regions receive much more and Metro Milwaukee remains close to the average. A very similar pattern is projected for the 2050s and 2080s and the regional trend is projected to become more prominent in the future.

- The Sen's slope results show the highest increasing trends in the northern and eastern parts of the study area. The Mann-Kendall test suggests that these regions show a significant trend.

- The study area receives much more precipitation in the summer than in the winter. The spatial variation of mean monthly observational data shows a unique spatial pattern for each month. In winter, spring and fall, the precipitation is highest in the southeast corner spreading into Metro Milwaukee, and the driest areas are found in the northwestern regions. In summer the driest areas are moving towards the northeastern parts, and the wettest areas are found in the southwest and west. A distinguished center of low precipitation over Metro Milwaukee occurs in May, September, October, and November.

- The projected spatial distribution of monthly precipitation for all three emission scenarios for the 2050s and 2080s is very similar to that of the current time period (1950-2006). The wettest areas in winter, fall, and spring are of slightly larger extent. The area with the lowest precipitation class of the study area, occurring over Metro Milwaukee, is also projected to be larger.

- An increase in mean monthly precipitation for the 2050s and 2080s is projected for winter, fall and spring. The projected changes in summer precipitation for the 2050s and 2080s show a decrease for all three emission scenarios.

- The 95th percentile precipitation for 1950-2006 ranges from 12 mm to 15 mm and is fairly homogenous throughout the study area. The spatial variation of 95th percentile precipitation is projected to increase between 16% to 40% for the 2050s, and between 16% to 46% for the 2080s depending on the emission scenario.

- The projected changes in extreme precipitation are higher than those simulated for the annual precipitation changes for both time periods and all three emission scenarios. The mean annual precipitation is projected to increase by 6% to 14% for the 2050s, and by 9% to 12% for the 2080s. The mean 95th percentile precipitation increases from 29% to 30% for the 2050s and the 2080s.

- The standard deviations for annual precipitation from the downscaling results of all three emission scenarios are higher than those from the observational data for 1950-2006 and the CGCM3 data for the base period 1961-1990. The analysis of annual precipitation for the base period showed a standard deviation of 126 mm for the observational data and 128 mm for the CGCM3 data. The analysis of the projected future annual precipitation revealed a range from 141 mm to 154 mm for the 2050s and from 144 mm to 152 mm for the 2080s. The standard deviations for the 95th percentile precipitation are nearly identical for the base period datasets and the downscaled future data.

- Based on the spatial patterns of annual and monthly precipitation, and the predominant wind direction, a pattern of higher precipitation amounts on the down-wind side of the city can be observed for the observational climate dataset from 1950-2006.

A more detailed analysis of the relationship between increased precipitation and wind direction is necessary to draw concrete conclusions if Metro Milwaukee causes an increase in precipitation amounts. The Metro Milwaukee does not seem to enhance the precipitation magnitude in the downwind side for all months. In some months (e.g. October) similar values of high precipitation can be found in the southern and northern regions, i.e. the highest occurring precipitation occurs in two places. This could either be due to a high variability in wind direction or that in these months the urban area does not have an effect on precipitation magnitude. In several months, May, September, October, and November an area of low precipitation over the Metro Milwaukee can be observed. This phenomenon might be dependent on the wind but could not be determined in this study. Therefore, an extensive wind analysis in connection to precipitation should be undertaken. This analysis should not only focus on the current time period but the future as well.

References

Barrow, Elaine M., and Rick J. Lee. 2000. *Climate Change and Environmental Assessment Part 2: Climate Change Guidance for Environmental Assessments.* The Canadian Institute for Climate Studies.

Carter, T. R., M. L. Parry, H. Harasawa, and S. Nishioka. 1994. *IPCC Technical Guidelines for Assessing Climate Change Impacts and Adaptations.* Geneva: Intergovernmental Panel on Climate Change.

Carter, T. R., K. Alfsen, E. Barrow, B. Bass, X. Dai, S. R. Desanker, F. Gaffin, et al. 2007. *General Guidelines on the Use of Scenario Data for Climate Impact and Adaptation Assessment.* Helsinki, Finland: Finnish Environmental Institute.

Changnon, S. A., R. G. Semonin, and F. A. Huff. 1976. A hypothesis for urban rainfall anomalies. *Journal of Applied Meteorology* 15 (6): 544-60.

Changnon, Stanley A. 1981. *METROMEX: A review and summary*. Vol. 18. Boston, MA: American Meteorological Society.

Changnon, Stanley A., and Floyd A. Huff. 1986. The urban-related nocturnal rainfall anomaly at St. Louis. *Journal of Climate and Applied Meteorology* 25 (12) (12/01): 1985-95.

Changnon, Stanley A., Robin T. Shealy, and Robert W. Scott. 1991. Precipitation changes in fall, winter, and spring caused by St. Louis. *Journal of Applied Meteorology* 30 (1) (01/01): 126-34.

Choi, Woonsup, Peter F. Rasmussen, Adam R. Moore, and Sung Joon Kim. 2009. Simulating streamflow response to climate scenarios in central Canada using a simple statistical downscaling method. *Climate Research* 40 : 89-102.

Diaz-Nieto, J., and R. L. Wilby. 2005. A comparison of statistical downscaling and climate change factor methods: Impacts on low flows in the river Thames, United Kingdom. *Climatic Change* 69 : 245-68.

Dixon, P. G., and Thomas L. Mote. 2003. Patterns and causes of Atlanta's urban heat island–initiated precipitation. *Journal of Applied Meteorology* 42 (9) (09/01): 1273-84.

Fowler, H. J., S. Blenkinsop, and C. Tebaldi. 2007. Linking climate change modelling to impacts studies: Recent advances in downscaling techniques for hydrological modelling. *International Journal of Climatology* 27 (12): 1547-78.

Fowler, H. J., and C. G. Kilsby. 2002. Precipitation and the north atlantic oscillation: A study of climatic variability in northern England. *International Journal of Climatology* 22 (7): 843-66.

Fuentes, U., and D. Heimann. 2000. An improved statistical-dynamical downscaling scheme and its application fo the alpine precipitation climatology. *Theoretical and Applied Climatology* 65 : 119-35.

Hanssen-Bauer, I., C. Achberger, R. E. Benestad, D. Chen, and E. J. Forland. 2005. Statistical downscaling of climate scenarios over Scandinavia. *Climate Research* 29 (3): 255-68.

Huff, F. A., and S. A. Changnon. 1973. Precipitation modification by major urban areas. *Bulletin of the American Meteorological Society* 54 (12) (12/01): 1220-32.

Huff, Floyd A., and Stanley A. Changnon. 1986. Potential urban effects on precipitation in the winter and transition seasons at St. Louis, Missouri. *Journal of Climate and Applied Meteorology* 25 (12): 1887-907.

IPCC. 2007a. *Climate Change 2007: Impacts, Adaptation and Vulnerability.* Contribution of working group II to the Fourth Assessment Report of the Intergovernmental Panel on Climate Change, 2007. eds. M. L. Parry, O. F. Canziani, J. P. Palutikof, P. J. van der Linden and C. E. Hanson. United Kingdom: Cambridge University Press.

———. 2007b. *Climate Change 2007: The Physical Science Basis. Contribution of Working Group I to the Fourth Assessment Report of the Intergovernmental Panel on Climate Change.* Cambridge, United Kingdom and New York, NY, USA: Cambridge University Press.

Jarvis, Claire H., and Neil Stuart. 2001. A comparison among strategies for interpolating maximum and minimum daily air temperatures. part I: The selection of guiding topographic and land cover variables. *Journal of Applied Meteorology* 40 (6): 1060-74.

Johnston, K., J. M. Ver Hoef, K. Krivoruchko, and N. Lucas. 2001. *Using ArcGIS^{TM} Geostatistical Analyst.* United States of America: ESRI, .

Kendall, M. G. 1975. *Rank Correlation Methods*. London, U.K.: Griffin.

Kucharik, C. J., S. P. Serbin, S. Varus, E. J. Hopkins, and M. M. Motew. 2010a. Patterns of climate change across Wisconsin from 1950 to 2006. *Physical Geography* 31 (1): 1-28.

Kucharik, C. J., D. J. Vimont, K. Holman, E. Hopkins, D. Lorenz, M. Notaro, S. Vavrus, and J. Young. 2010b. *Climate Change in Wisconsin.* Wisconsin Initiative on Climate Change Impacts.

Leander, Robert, and T. Adri Buishand. 2007. Resampling of regional climate model output for the simulation of extreme river flows. *Journal of Hydrology* 332 : 487-96.

Manly, Bryan F. J. 2009. *Statistics for Environmental Science and Management*. Boca Raton: CRC Press.

Mann, H. B. 1945. Nonparametric tests against trend. *Econometrica* 13 : 245-59.

Maraun, D., F. Wetterhall, A. M. Ireson, R. E. Chandler, E. J. Kendon, M. Widmann, S. Brienen, et al. 2010. Precipitation downscaling under climate change: Recent developments to bridge the gap between dynamical models and the end user. *Reviews of Geophysics* 48 (3) (09/24): RG3003.

Midwestern Regional Climate Center. Climate change and variability in the Midwest. in Midwest Regional Climate Center [database online]. 2009. Available from htpp://mcc.sws.uiuc.edu/climate_midwest/mwclimate_change.htm.

Mitchell, J. M., B. Dzerdzeevskii, H. Flohn, W. L. Hofmeyr, H. H. Lamb, K. N. Rao, and C. C. Wallen. 1966. *Climatic Change.* Geneva, Switzerland: Secretariat of the World Meteorological Organization.

Nakicenovic, N., J. Alcamo, G. Davis, B. de Vries, J. Fenhann, S. Gaffin, K. Gregory, et al. 2000. *IPCC Special Report on Emissions Scenarios.* Cambridge: Cambridge University Press.

Nalder, I. A., and R. W. Wein. 1998. Spatial interpolation of climatic normals: Test of a new method in the Canadian boreal forest. *Agricultural and Forest Meteorology* 92 : 211-25.

Olsson, J., K. Berggren, M. Olofsson, and M. Viklander. 2009. Applying climate model precipitation scenarios for urban hydrological assessment: A case study in Kalmar City, Sweden. *Atmospheric Research* 92 (3): 364-75.

Prudhomme, C., N. Reynard, and S. Crooks. 2002. Downscaling of global climate models for flood frequency analysis: Where are we now? *Hydrological Processes* 16 : 1137-50.

Schlünzen, K. H., P. Hoffmann, G. Rosenhagen, and W. Riecke. 2010. Long-term changes and regional differences in temperature and precipitation in the metropolitan area of Hamburg. *International Journal of Climatology* 30 (8): 1121-36.

Semenov, M. A., and P. Stratonovitch. 2010. Use of multi-model ensembles from global climate models for assessment of climate change impacts. *Climate Reearchs* 41 (1): 1-14.

Sen, Pranab Kumar. 1968. Estimates of the regression coefficient based on Kendall's tau. *Journal of the American Statistical Association* 63 (324) (Dec.): pp. 1379-1389.

Serbin, S. P., and C. J. Kucharik. 2009. Spatiotemporal mapping of temperature and precipitation for the development of a multidecadal climatic dataset for Wisconsin. *Journal of Applied Meteorology and Climatology* 48 (4): 742-57.

Shepherd, J. M. 2005. A review of current investigations of urban-induced rainfall and recommendations for the future. *Earth Interactions* 9 (12) (07/01): 1-27.

Shepherd, J. M., Harold Pierce, and Andrew J. Negri. 2002. Rainfall modification by major urban areas: Observations from spaceborne rain radar on the TRMM satellite. *Journal of Applied Meteorology* 41 (7) (07/01): 689-701.

Smith, J. B., and M. Hulme. 1998. Climate change scenarios. In *UNEP Handbook on Methods for Climate Change impact Assessment and Adaptation Studies.*, eds. I. Burton, J. F. Feenstra, J. B. Smith and R. S. J. Tol. Version 2.0 ed., 3-1-3-40. Vrije Universiteit, Amsterdam: United Nations Environment Programme and Institute for Environmental Studies.

Sunyer, M. A., H. Madsen, and P. H. Ang. 2012. A comparison of different regional climate models and statistical downscaling methods for extreme rainfall estimation under climate change. *Atmospheric Research* 103: 119-28.

Toreti, A., G. Fioravanti, W. Perconti, and F. Desiato. 2009. Annual and seasonal precipitation over Italy from 1961 to 2006. *International Journal of Climatology* 29: 1976-87.

Wilby, R. L., S. P. . Charles, E. Zorita, B. Timbal, P. Whetton, and L. O. Mearns. 2004. *Guidlines for Use of Climate Scenarios Developed from Statistical Downscaling Methods.*

Wilby, R. L., and T. M. L. Wigley. 1997. Downscaling general circulation model output: A review of methods and limitations. *Progress in Physical Geography* 21 (4): 530-48.

Wilks, D. S., and R. L. Wilby. 1999. The weather generation game: A review of stochastic weather models. *Progress in Physical Geography* 23 (3): 329-57.

Wisconsin Initiative on Climate Change Impact. 2011. *Wisconsin's Changing Climate: Impacts and Adaptation*. Madison, Wisconsin: Nelson Institute for Environmental

Studies, University of Wisconsin-Madison and the Wisconsin Departnment of Natural Resources.

Xu, C. -y. 1999. From GCMs to river flow: A review of downscaling methods and hydrologic modelling approaches. *Progress in Physical Geography* 23 (2): 229-49.

Xu, C. -Y, E. Widen, and S. Halldin. 2005. Modelling hydrological consequences of climate change - progress and challenges. *Advances in Atmospheric Sciences* 22 (6): 789-97.

Zhang, Q., C. -Y Xu, Z. Zhang, Y. D. Chen, and C. -L Liu. 2009. Spatial and temporal variability of precipitation over China, 1951-2005. *Theoretical and Applied Climatology* 95: 53-68.

Zhang, Qiang, Tong Jiang, Marco Gemmer, and Stefan Becker. 2005. Precipitation, temperature and runoff analysis from 1950 to 2002 in the Yangtze basin, China. *Hydrological Sciences "Journal-Des Sciences Hydrologiques* 50 : 65-80.

Appendix - MATLAB Function for the Delta Method

This function is based on that used in the study by Choi et al. (2009).

The inputs needed for this function are:
 Pobs: Matrix of observed precipitation at a station, without 29
 February
 Pgcm_c: Matrix of GCM-simulated precipitation for current climate
 Pgcm_f: Matrix of GCM-simulated precipitation for future climate

 Output is given as:
 Pf: Matrix of future precipitation

```matlab
function [Pf] = p_scenario(Pobs, Pgcm_c, Pgcm_f)
d = cumsum([1 31 28 31 30 31 30 31 31 30 31 30 31]);
Pscenario = zeros(size(Pobs));
 for i=1:12
    Po = Pobs(:,d(i):d(i+1)-1);
    Po = Po(:);
    Pc = Pgcm_c(:,d(i):d(i+1)-1);
    Pc = Pc(:);
    Pf = Pgcm_f(:,d(i):d(i+1)-1);
    Pf = Pf(:);
    EPf = mean(Po) * (mean(Pf)/mean(Pc));
    r = length(find(Po==0))/length(Po);
    TPo = sortrows(Po); TPo(1:floor(r*length(TPo))) = [];
    TPc = sortrows(Pc); TPc(1:floor(r*length(TPc))) = [];
    TPf = sortrows(Pf); TPf(1:floor(r*length(TPf))) = [];
    SPf = std(TPo) * std(TPf)/std(TPc);
    par0 = [mean(Pf)/mean(Pc) , 1];
    par = fminsearch(@(x) obj1(x,Po,EPf,SPf), par0);
    fprintf(1,'\n Month %2d %6.2f %6.2f %6.3f %6.3f %6.3f
%6.3f',...
        i,par(1),par(2),EPf, mean(par(1)*Po.^par(2)),SPf,
std(par(1)*Po.^par(2)))
    Pscenario(:,d(i):d(i+1)-1) = par(1)*Pobs(:,d(i):d(i+1)-
1).^par(2);
end
[Pf] = Pscenario;


function f = obj1(par,P,EPf,SPf)
Pf = par(1).*P.^par(2);
f = abs(mean(Pf)-EPf) + abs(std(Pf)-SPf);
```